OH, HO_2, and RO_2 radical chemistry in a rural forest environment: Measurements, model comparisons, and evidence of a missing radical sink

Brandon Bottorff[1], Michelle M. Lew[1a], Youngjun Woo[1], Pamela Rickly[2b], Matthew D. Rollings[3c], Benjamin Demming[3d], Daniel C. Anderson[4e], Ezra Wood[4], Hariprasad D. Alwe[5f], Dylan B. Millet[5], Andrew Weinheimer[6], Geoff Tyndall[6], John Ortega[6], Sebastien Dusanter[7], Thierry Leonardis[7], James Flynn[8], Matt Erickson[8], Sergio Alvarez[8], Jean C. Rivera-Rios[9g], Joshua D. Shutter[9h], Frank Keutsch[9], Detlev Helmig[10], Wei Wang[11], Hannah M. Allen[12], Johnathan H. Slade[13i], Paul B. Shepson[13,14j], Steven Bertman[15], and Philip S. Stevens[1,2]

[1] Department of Chemistry, Indiana University, Bloomington, IN 47405, USA
[2] O'Neill School of Public and Environmental Affairs, Indiana University, Bloomington, IN 47405, USA
[3]Department of Chemistry, University of Massachusetts, Amherst, MA 01003, USA
[4]Department of Chemistry, Drexel University, Philadelphia, PA 19104, USA
[5]Department of Soil, Water, and Climate, University of Minnesota, Twin Cities, Saint Paul, MN 55108, USA
[6]National Center for Atmospheric Research, Boulder, CO, 80305 USA
[7]IMT Nord Europe, Institut Mines- Télécom, Univ. Lille, Center for Energy and Enivronment, F-59000 Lille, France
[8]Department of Earth and Atmospheric Sciences, University of Houston, Houston, TX 77004, USA
[9]Department of Chemistry and Chemical Biology, Harvard University, Cambridge, MA 02138, USA
[10]Boulder A.I.R. LLC, Boulder, CO 80305 USA
[11]Institute of Arctic and Alpine Research, University of Colorado, Boulder, CO 80309, USA
[12]Division of Chemistry and Chemical Engineering, California Institute of Technology, Pasadena, CA 91125, USA
[13]Department of Chemistry, Purdue University, West Lafayette, IN 47907, USA
[14]Department of Earth, Atmospheric, and Planetary Sciences, Purdue University, West Lafayette, IN 47907, USA
[15]Institute of the Environment and Sustainability, Western Michigan University, Kalamazoo, MI, 49008, USA

[a] now at: California Air Resources Board, Sacramento, CA 95814, USA
[b] now at: Colorado Department of Public Health and Environment, Denver, CO 80246, USA
[c] now at: Dept. of Chemistry, University of California, Berkeley CA 94720, USA
[d] now at: Dept. of Chemistry, Smith College, Northampton MA 01063, USA
[e] now at: GESTAR II, University of Maryland Baltimore County, Baltimore, MD 21228, USA
[f] now at: Forschungszentrum Jülich, Institute of Energy and Climate Research, Troposphere (IEK-8), Jülich, Germany
[g] now at: School of Chemical & Biomolecular Engineering, Georgia Institute of Technology, Atlanta, GA 30332 USA
[h] now at: Department of Soil, Water and Climate, University of Minnesota, St. Paul, MN 55108, USA
[i] now at: Department of Chemistry and Biochemistry, University of California San Diego, La Jolla, CA 92093, USA
[j] now at: School of Marine and Atmospheric Sciences, Stony Brook University, Stony Brook, NY 11794, USA

Correspondence to: Brandon Bottorff (brapbott@indiana.edu); Philip S. Stevens (pstevens@indiana.edu)

Abstract.

The hydroxyl (OH), hydroperoxy (HO_2), and organic peroxy (RO_2) radicals play important roles in atmospheric chemistry. In the presence of nitrogen oxides (NO_x), reactions between OH and volatile organic compounds (VOCs) can initiate a radical propagation cycle that leads to the production of ozone and secondary organic aerosols. Previous measurements of these radicals under low-NO_x conditions in forested environments characterized by emissions of biogenic VOCs, including isoprene and monoterpenes, have shown discrepancies with modeled concentrations.

During the summer of 2016, OH, HO_2 and RO_2 radical concentrations were measured as part of the Program for Research on Oxidants: Photochemistry, Emissions, and Transport – Atmospheric Measurements of Oxidants in Summer (PROPHET-AMOS) campaign in a mid-latitude deciduous broadleaf forest. Measurements of OH and HO_2 were made by laser-induced fluorescence – fluorescence assay by gas expansion techniques (LIF-FAGE) and total peroxy radical (XO_2) mixing ratios were

measured by an ethane chemical amplification (ECHAMP) instrument. Supporting measurements of photolysis frequencies, VOCs, NO_x, O_3, and meteorological data were used to constrain a zero-dimensional box model utilizing either the Regional Atmospheric Chemical Mechanism (RACM2), or the Master Chemical Mechanism (MCM). Model simulations tested the influence of HO_x regeneration reactions within the isoprene oxidation scheme from the Leuven Isoprene Mechanism (LIM1). On average, the LIM1 models overestimated daytime maximum measurements by approximately 40% for OH, 65% for HO_2, and more than a factor of two for XO_2. Modelled XO_2 mixing ratios were also significantly higher than measured at night. Addition of $RO_2 + RO_2$ accretion reactions for terpene-derived RO_2 radicals to the model can partially explain the discrepancy between measurements and modelled peroxy radical concentrations at night but cannot explain the daytime discrepancies when OH reactivity is dominated by isoprene. The models also overestimated measured concentrations of isoprene-derived hydroxyhydroperoxides (ISOPOOH) by a factor of ten during the daytime, consistent with the model overestimation of peroxy radical concentrations. Constraining the model to the measured concentration of peroxy radicals improves the agreement with the measured ISOPOOH concentrations, suggesting that the measured radical concentrations are more consistent with the measured ISOPOOH concentrations. These results suggest that the models may be missing an important daytime radical sink and could be overestimating the rate of ozone and secondary product formation in this forest.

1 Introduction

As a dominant oxidant in the lower troposphere, the hydroxyl radical (OH) initiates reactions with volatile organic compounds (VOCs) leading to the production of hydroperoxy radicals (HO_2) and organic peroxy radicals (RO_2). In the presence of nitrogen oxides ($NO_x = NO + NO_2$), reactions of these radicals establish a fast cycle that can produce ozone and secondary organic aerosols (SOA). Given their central role in atmospheric chemistry, an accurate understanding of radical chemistry is important to address current issues of air quality and climate change. Because of their short atmospheric lifetimes, measurements of these radicals can provide a test of our understanding of this complex chemistry, including our knowledge of radical sources, sinks, and propagation pathways (Heard and Pilling, 2003).

Several field campaigns have been conducted to investigate radical concentrations in both urban and forested environments. Although measurements of OH concentrations in urban areas have been generally consistent with model predictions (Ren et al., 2003; Shirley et al., 2006; Kanaya et al., 2007a; Dusanter et al., 2009b; Lu et al., 2013; Griffith et al., 2016; Tan et al., 2017; Tan et al., 2018; Tan et al., 2019; Whalley et al., 2021) measurements of peroxy radicals in such environments have generally been underpredicted by atmospheric models (Griffith et al., 2016; Baier et al., 2017; Tan et al., 2017; Whalley et al., 2021). Measurements in forested regions characterized by low NO_x mixing ratios and elevated emissions of biogenic VOCs, such as isoprene and monoterpenes, have indicated discrepancies with modelled results, with several observations of higher-than-expected OH concentrations in isoprene-rich environments (Tan et al., 2001; Lelieveld et al., 2008; Hofzumahaus et al., 2009; Whalley et al., 2011; Lu et al., 2012; Rohrer et al., 2014). However, several recent studies have revealed potential interferences with measurements of OH radicals in forested environments (Mao et al., 2012; Novelli et al., 2014b; Feiner et al., 2016; Lew et al., 2020). Accounting for these interferences resulted in measured OH concentrations that were in good agreement with model predictions in these forested areas.

In contrast, measurements of HO_2 and RO_2 radical concentrations in forested areas have shown variable agreement with model predictions. In these environments, measured HO_2 concentrations were sometimes found to agree with model predictions (Tan et al., 2001; Ren et al., 2006; Feiner et al., 2016; Tan et al., 2017), but were sometimes lower (Carslaw et al., 2001; Kanaya et al., 2007b; Whalley et al., 2011; Kanaya et al., 2012; Mao et al., 2012; Griffith et al., 2013; Mallik et al., 2018), or higher than

model predictions (Carslaw et al., 2001; Kubistin et al., 2010; Kim et al., 2013; Hens et al., 2014). Part of this variability may be due to measurement interferences from certain RO_2 radicals in systems that detect HO_2 through the conversion to OH using the $HO_2 + NO \rightarrow OH + NO_2$ reaction (Fuchs et al., 2011; Whalley et al., 2013; Hens et al., 2014; Crowley et al., 2018; Lew et al., 2018). However, the extent of RO_2 radical contributions to HO_2 measurements in many of the earlier campaigns mentioned above is not clear. While accounting for this interference would improve agreement when the model underestimates HO_2, it would worsen agreement in the case of an overestimation.

The discrepancies between measured and modeled radical concentrations in forest environments brings into question our understanding of the chemistry of biogenic VOCs (BVOCs) and their contribution to the production of ozone and SOA in the atmosphere. Isoprene is of particular importance due to its global abundance and high reactivity with the OH radical (Wennberg et al., 2018). Current models suggest that emissions of isoprene alone account for half of global non-methane VOC emissions (Guenther et al., 2012; Wennberg et al., 2018). Several theoretical and laboratory studies have investigated the atmospheric chemistry of isoprene and its oxidation products, revealing that isomerization of isoprene-based peroxy radicals and subsequent product pathways could recycle OH and HO_2 radicals resulting in higher radical concentrations under low-NO_x conditions (Fuchs et al., 2013; Peeters et al., 2014; Liu et al., 2017; Wennberg et al., 2018; Medeiros et al., 2022).

In addition to isoprene, other biogenic VOCs, including monoterpenes, can play a significant role in the overall oxidative capacity of some environments. Globally, monoterpene emissions are estimated to be more than 100 Tg yr^{-1} and constitute as much as 10% of BVOC emissions (Sindelarova et al., 2014). While emissions of isoprene are strongly dependent on photosynthetic photon flux as well as temperature, several plant species emit monoterpenes also under dark conditions (Harley et al., 1996; Owen et al., 2002). Similar to the chemical mechanism of isoprene oxidation, peroxy radicals produced from the oxidation of monoterpenes can undergo isomerization reactions as part of autooxidation mechanisms, leading to the production of highly-oxidized peroxy radical products (Jokinen et al., 2014). Under low-NO_x conditions, these reactions can compete with reaction with NO as well as with peroxy radical self and cross reactions.

While it is known that self- and cross-reactions of RO_2 can form either alkoxy radicals (reaction R1) or an alcohol and a carbonyl species (R2) (Orlando and Tyndall, 2012), a third pathway that leads to the formation of a dimeric dialkyl peroxide (R3) has been proposed but previously regarded as less significant due to low yields for small RO_2 species (Lightfoot et al., 1992; Tyndall et al., 2001; Noell et al., 2010). However, recent studies have observed the formation of gas phase C_{19}-C_{20} dimer compounds and suggest that autoxidation and $RO_2 + RO_2$ reactions between terpene-derived peroxy radicals may form low-volatility accretion products (R3) (Crounse et al., 2013; Ehn et al., 2014; Berndt et al., 2018a; Berndt et al., 2018b; Bianchi et al., 2019).

$$RO_2 + R'O_2 \longrightarrow RO + R'O + O_2 , \quad \text{(R1)}$$

$$RO_2 + R'O_2 \longrightarrow ROH + R'C{=}O + O_2 , \quad \text{(R2)}$$

$$RO_2 + R'O_2 \longrightarrow ROOR' + O_2 , \quad \text{(R3)}$$

In addition to significantly affecting of SOA formation, these reactions could be relevant alongside reactions with NO_x or HO_2 as radical termination reactions and should be considered when modelling radical concentrations in low-NO_x regions characterized by significant biogenic VOC emissions.

This study presents measurements of OH, HO_2, and total peroxy radical ($XO_2 = RO_2 + HO_2$) concentrations made within a remote forested region during the PROPHET-AMOS 2016 (Program for Research on Oxidants: Photochemistry, Emissions, and Transport – Atmospheric Measurements of Oxidants in Summer) field campaign. The measurements are compared to predicted radical concentrations from zero-dimensional box models constrained to a wide range of trace gases and meteorological conditions.

Additional model simulations that incorporate the Leuven Isoprene Mechanism (LIM1) for isoprene degradation and a series of $RO_2 + R'O_2$ reactions that form accretion products are accompanied by a radical budget analysis to test current atmospheric chemistry mechanisms and investigate the fate of isoprene- and monoterpene-derived peroxy radicals in this low-NOx environment.

2 Experimental Methods

2.1 PROPHET-AMOS measurement site

All measurements described below were performed as part of the PROPHET-AMOS 2016 field campaign. Measurements were conducted throughout the month of July at the PROPHET facility at the University of Michigan Biological Station (UMBS) in northern Michigan (45.5588° N, 84.7145° W). The mixed deciduous and coniferous forest site consists primarily of isoprene-emitting species such as big-tooth aspen and red oak but also monoterpene-emitting species such as red maple, white pine, and paper birch (Ortega et al., 2007; Bryan et al., 2015). The site has been described in more detail elsewhere (Carroll et al., 2001; Ortega et al., 2007; Griffith et al., 2013). The majority of the measurements described below were performed near the top of the 31-m tower, approximately 10 m above the forest canopy either by placing the instrument directly on the top of the tower, sampling from a glass manifold in the laboratory that pulled air from the top of the tower, or by sampling from individual inlets from the top of the tower. Measurements of ozone were taken from the top of the nearby Ameriflux tower, which is 100 m to the north of the PROPHET tower. Table 1 summarizes the measurements used in this study.

Table 1: Measured species used for data analysis and model calculations and respective measurement techniques.

Measured Species	Instrument	Technique	Reference	LOD
OH, HO_2	LIF-FAGE	Laser-induced fluorescence-fluorescence assay by gas expansion	(Dusanter et al., 2009a; Griffith et al., 2013)	OH - 6.5×10^5 cm^{-3} (2 hour) HO_2 - 1.1×10^7 cm^{-3} (0.4 ppt) (20 s)
XO_2	ECHAMP	Ethane Chemical amplification	(Wood and Charest, 2014; Wood et al., 2017)	1-3 ppt (2 min)
NO, NO_2	2-channel chemiluminescence	Chemiluminescence and LED converter for NO_2	NCAR (Ridley and Grahek, 1990)	1-2 ppt (10 s)
O_3	Thermo Scientific 49C	UV absorbance		1.0 ppb
VOCs	PTR-Qi-ToF	Proton Transfer Reaction-Time-of-Flight Mass Spectrometry	(Millet et al., 2018)	
NMHCs	Online GC/FID/FID	Gas chromatography with flame ionization detection	(Badol et al., 2004)	10-100 ppb (1.5 h)
OVOCs	DNPH-HPLC	dinitrophenylhydrazine cartridges and offline high performance liquid chromatography and UV detection		
jNO_2		spectral radiometry	(Shetter and Müller, 1999)	0.3×10^{-4} s^{-1}
ISOPOOH	GC-HRToF-CIMS	Low-pressure gas chromatography coupled with high-resolution time-of-flight chemical ionization mass spectrometry	(Vasquez et al., 2018)	~10 ppt
IHN	CIMS	Iodide-adduct chemical ionization mass spectrometry	(Xiong et al., 2015)	~10 ppt

During the campaign, isoprene, the sum of methylvinylketone and methacrolein, monoterpenes, acetaldehyde, and other VOCs and oxygenated VOCs (OVOCs) were measured by the University of Minnesota using proton transfer reaction-quadrupole interface time-of-flight mass spectrometry (PTR-QiTOF) (Millet et al., 2018). In addition, C2–C10 alkanes and alkenes, butadiene, C6–C9 aromatic compounds, and isoprene were measured by IMT Nord Europe using a thermal desorption gas chromatography with flame ionization detection (GC-FID) instrument with a 1.5-h time resolution, while C_2–C_{10} aldehydes, C_2–C_6 ketones, and C_2–C_4 alcohols were measured by thermal desorption GC-FID with mass spectrometry (GC-FID-MS) with a 1.5-h time resolution (Badol et al., 2004; Roukos et al., 2009). NO and NO_2 were measured by the NCAR single-channel chemiluminescence instrument (Ridley and Grahek, 1990), ozone was measured by UV absorption by the University of Colorado, and CO by laser-based off-axis integrated cavity output spectroscopy (Los Gatos Research) by the University of Houston and Rice University groups. Isoprene hydroxy hydroperoxides (ISOPOOH) were measured using a gas chromatograph chemical ionization mass spectrometer (GC-ToF-CIMS) by Caltech (Vasquez et al., 2018). Isoprene hydroxy nitrates were measured by an iodine-adduct chemical ionization mass spectrometer by Purdue University (Xiong et al., 2015). Photolysis frequencies were measured using spectral radiometry (Shetter and Müller, 1999) by the University of Houston. Measurements of OH, HO_2 and XO_2 radicals are described in detail below.

2.2 Measurements of HO_x concentrations

Both OH and HO_2 were measured using the Indiana University laser-induced fluorescence-fluorescence assay by gas expansion (IU-FAGE) instrument that has been described in more detail previously (Dusanter et al., 2009a; Griffith et al., 2013; Lew et al., 2020). Briefly, OH radicals are detected by laser-excitation at 308 nm and subsequent fluorescence detection also at 308 nm. The sampled air expands into a low-pressure cell, which extends the OH fluorescence lifetime by reducing the concentration of species that may quench OH fluorescence and allows temporal filtering of OH fluorescence from more intense scattered laser light (Heard and Pilling, 2003).

The IU-FAGE laser system used in this study consisted of a Spectra Physics Navigator II YHP40-532Q that produced approximately 7.5 W of 532-nm radiation (10-kHz repetition rate) to pump a Sirah Credo dye laser (255 mg/L of Rhodamine 610 and 80 mg/L of Rhodamine 101 in ethanol) resulting in approximately 40 mW of radiation that is tunable near 308 nm. This laser system was housed in the laboratory at the bottom of the PROPHET measurement tower and 308-nm radiation was focused onto the entrance of a 50-m optical fiber to transmit the laser emission to the sampling cell.

The IU-FAGE sampling cell was located atop the 31-m measurement tower, approximately 10 meters above the forest canopy. Ambient air was drawn into the detection cell through a pinhole inlet (0.64 mm diameter) by means of three scroll pumps (Edwards XDS 35i) connected in parallel. The pumps were located at the bottom of the tower and connected to the sampling cell by two parallel 3.8-cm inner-diameter vacuum hoses, which resulted in a sampling cell pressure of 0.6 kPa (4.5 torr) and a flow of 3 SLPM through the sampling inlet.

On average, approximately 1.25 mW of 308-nm radiation exited the 50-m fiber and entered the sampling cell during the campaign. The laser emission enters the sampling cell perpendicular to the sampled air mass and intersects the expanded air in a White cell configuration with approximately 24 passes. The OH fluorescence is collected along an axis that is orthogonal to both the laser beam and sampled air mass and detected using a microchannel plate photomultiplier tube (MCP-PMT) detector (Hamamatsu R5946U), a preamplifier (Stanford Research Systems SR445), and a photon counter (Stanford Research Systems SR400). The MCP-PMT is turned off and the photon counter is inactive during the laser pulse by means of a delay generator (Berkley Nucleonics 565) to allow the OH fluorescence to be temporally filtered from scattered laser light.

The net OH fluorescence signal is determined through successive spectral-modulation cycles in which the dye laser emission wavelength is tuned on- and off- resonance with the $Q_1(3)$ transition of OH near 308 nm. A background signal, which primarily consists of scattered laser light that extends into the detection window, is established by tuning the laser emission off-resonance with the OH transition, and therefore not exciting OH radicals. This background signal is subtracted from on-resonance signal. A reference cell in which OH is generated by the thermal dissociation of water vapor is used to ensure maximum overlap between dye-laser emission and the OH transition wavelength.

The IU-FAGE measurements of OH are subject to potential interferences when OH radicals are generated inside the detection cell. In the presence of water vapor, the photolysis of ozone by the laser can produce hydroxyl radicals through reactions R4 and R5 (Davis et al., 1981a; Davis et al., 1981b).

$$O_3 + h\nu\ (< 340\ \text{nm}) \rightarrow O(^1D) + O_2\ , \qquad \text{(R4)}$$

$$O(^1D) + H_2O \rightarrow OH + OH, \qquad \text{(R5)}$$

To characterize this and any other interference, a chemical scrubbing technique is used to remove ambient OH prior to entering the detection cell (Griffith et al., 2016; Rickly and Stevens, 2018; Lew et al., 2020). This chemical modulation technique is used to monitor levels of the laser-generated ozone-water interference and any other interference that may produce OH radicals inside the detection cell. Hexafluoropropylene (C_3F_6, 95.5% in N_2; Matheson Gas) was added through a circular injector 1 cm above the

inlet with a flow rate of approximately 3.5 sccm to remove 95% of external OH radicals (Rickly and Stevens, 2018). The differences between the measured OH during C_3F_6 addition and OH measurements including the interference represent the net ambient OH concentration in the atmosphere. The addition of C_3F_6 is modulated in between ambient OH measurements every 15 min for a duration of 10 min.

Measurements of HO_2 were made indirectly after addition of NO to the sampled air mass to convert ambient HO_2 to OH through the fast $HO_2 + NO \rightarrow OH + NO_2$ reaction. A small flow (approximately 2 sccm) of NO (Matheson, 1% in nitrogen) was added to the sampled air mass through a Teflon loop injector that was positioned directly below the sampling inlet, resulting in an added NO concentration of approximately 9×10^{11} cm^{-3}. The fraction of HO_2 converted into OH was measured during calibration experiments performed during and after the campaign and was 14.0 ± 3.2%. This low NO concentration minimized the impact of interferences from RO_2 radicals derived from the OH-initiated oxidation of alkenes and aromatics that can be quickly converted to HO_2 (Fuchs et al., 2011; Lew et al., 2018). The high conversion efficiencies reported for these RO_2 radicals is due to the rapid decomposition of β-hydroxyalkoxy radicals that are formed from the RO_2 + NO reaction. This decomposition forms a hydroxyalkyl radical that reacts rapidly with O_2 to produce HO_2 in the detection cell. This can lead to the detection of both HO_2 and a fraction of RO_2 radicals denoted as HO_2^* ($HO_2^* = HO_2 + \alpha RO_2$, $0<\alpha<1$). Calibrations before and after the campaign similar to those described in Lew et al. (2018) indicated that the low NO concentration injected into the detection cell (approximately 9×10^{11} cm^{-3}) resulted in an RO_2-to-HO_2 conversion efficiency of approximately 10% for isoprene-based peroxy radicals and an RO_2-to-OH conversion efficiency of less than 2% (Fig. S1). As a result, the HO_2 measurements were performed at the low NO flow that effectively minimized the impact of any potential interference from isoprene-derived RO_2 species that are dominant during the day at the PROPHET site (Griffith et al., 2013).

The instrument was calibrated by producing known concentrations of OH and HO_2 from the photolysis of water vapor in air as described by Dusanter et al. (2008). The calibration source consists of an aluminum flow reactor with quartz windows on two opposite sides. Aluminum cartridges adjacent to each window house a low-pressure mercury pen lamp and a photodiode detector, both of which are continuously purged with dry nitrogen to stabilize the lamp-temperature and prevent light absorption by atmospheric gases. Radiation from the mercury lamp passes through a bandpass filter centered at 185 nm prior to illuminating the flow reactor and detector. The location of the mercury lamp and photodiode is adjustable along the length of the calibration source to allow for the measurement of radical surface loss between the illuminated region and the exit of the calibrator. For calibrations during PROPHET, zero air was delivered to the calibration source at a flow rate of 50 L min^{-1}. A variable fraction of the flow (5 – 40%) was diverted through a set of custom bubblers containing high purity water at the base of the tower. This humidified fraction of air was mixed back with the initial flow in approximately 35 m of PTFE tubing (1.25 cm i.d.) before entering the calibration source. Calibrations were performed before, after, and intermittently during the campaign to track changes in sensitivity (Dusanter et al., 2008). The uncertainty associated with this calibration technique is approximately 18% (1σ) for both OH and HO_2.

As previously mentioned, a 50-m fiber optic cable was used to transmit laser radiation to the sampling cell for the above-canopy measurements. The long fiber presented technical challenges that impacted the performance of the IU-FAGE instrument. Due to the length of the fiber, the laser pulse was temporally broadened prior to entering the detection cell and resulted in an increase of background laser scatter of the instrument. This broadened pulse made temporal filtering of scattered laser light difficult, and ultimately led to a lower sensitivity and a higher limit of detection for OH. In addition, the length of the fiber corresponded to a decrease in transmission of radiation through the fiber. An average transmission of 8% led to 0.76-2.15 mW of 308 nm radiation in the detection cell over the course of the campaign. Due to low laser power and high background signal, long averaging times were necessary for OH measurements. The limit of detection for OH was 6.5×10^5 molecules cm^{-3} (1σ, 2-hour

average). Measurements of HO_2 were performed approximately once per hour with a limit of detection of 1.1×10^7 cm^{-3} (0.4 ppt) (1σ, 20-s average).

2.3 Measurements of Total Peroxy Radicals (XO_2)

Total peroxy radicals were measured by an Ethane Chemical Amplifier (ECHAMP) instrument that has been previously described in detail (Wood et al., 2017). This instrument is similar to traditional chemical amplifiers that mix ambient air with excess CO and NO (Cantrell and Stedman, 1982; Hastie et al., 1991; Cantrell et al., 1996), but instead utilizes chemical amplification by ethane (C_2H_6) and NO followed by detection of NO_2 using cavity-attenuated phase-shift (CAPS) spectroscopy.

The ECHAMP inlet box was positioned on the top platform of the tower at a height of 31 m. Ambient air was sampled at a flow rate of 7.3 SLPM through a 0.4 cm inner diameter (ID) glass inlet that was internally coated with halocarbon wax to minimize radical loss on surfaces. A small flow (0.35 SLPM) of pure O_2 was added through a side port to this main flow. The O_2 addition increases the O_2 mixing ratio in the sampled air to 24.6% and reduces both the value and the variability of the relative humidity in the sampled air. The sampled air finally entered two reaction chambers at individual flow rates of 1.0 L min^{-1} with the remaining sampled air used to monitor temperature and RH. In the amplification chamber, the sampled air was immediately mixed with 20 sccm of 50 ppm NO and 20 sccm of 50% C_2H_6 through an upstream reagent addition port, leading to final mixing ratios for NO and C_2H_6 of 1 ppm and 1% respectively. A flow of 20 sccm N_2 was added downstream, 100 ms later. In this chamber, RO_x species are converted to HO_2 and OH through reactions with NO (R6 – R8). Reactions (R8 – R12) repeat several times leading to the formation of NO_2 that is subsequently measured by a CAPS monitor.

$$RO_2 + NO \longrightarrow RO + NO_2\,, \quad \text{(R6)}$$

$$RO + O_2 \longrightarrow HO_2 + \text{products}, \quad \text{(R7)}$$

$$HO_2 + NO \longrightarrow OH + NO_2, \quad \text{(R8)}$$

$$OH + C_2H_6 \longrightarrow C_2H_5 + H_2O, \quad \text{(R9)}$$

$$C_2H_5 + O_2 + M \longrightarrow C_2H_5O_2 + M, \quad \text{(R10)}$$

$$C_2H_5O_2 + NO \longrightarrow C_2H_5O + NO_2\,, \quad \text{(R11)}$$

$$C_2H_5O + O_2 \longrightarrow CH_3CHO + HO_2, \quad \text{(R12)}$$

In the background chamber, the sampled air was first mixed with NO and N_2, and then C_2H_6 was added 100 ms later. In this mode, ambient radicals are removed by successive reactions with NO (R6 – R8) until they form HONO via the OH + NO → HONO reaction, and therefore amplification chemistry does not occur. After reagent addition, air from each chamber enters identical CAPS monitors. The CAPS NO_2 measurements from the background chamber represent ambient NO_2, NO_2 from the reaction of ambient O_3 with added NO, and NO_2 from reactions of ambient peroxy radicals with NO, but not from ethane amplification reactions. The CAPS NO_2 monitor following the amplification chamber measures the sum of that observed from the background chamber and NO_2 produced from amplification reactions (ΔNO_2) is determined from the difference between the amplification and background chambers. The concentration of peroxy radicals is calculated by dividing [ΔNO_2] by the experimentally determined amplification factor, *F*.

$$[RO_x] = \Delta[NO_2]_{(CAPS_{RO_x} - CAPS_{O_x})}/F, \quad (1)$$

The amplification factor was determined as a function of relative humidity by producing known concentrations of peroxy radicals with two different calibration sources. The first source relies on the photolysis of water vapor method which is similar to that described above for the IU-FAGE instrument and is commonly used to calibrate other chemical amplifiers (Mihele and Hastie, 2000; Horstjann et al., 2014) and LIF-FAGE instruments (Heard and Pilling, 2003; Dusanter et al., 2008). This method produces equivalent concentrations of OH and HO_2 that are quantified by O_2 actinometry and measured concentrations of H_2O and O_3 in the calibration gas, and OH can be quantitatively converted to HO_2 or isoprene peroxy radicals through the addition of H_2 or isoprene, respectively. The second calibration source was based on the photolysis of methyl iodide (CH_3I) at 254-nm to produce CH_3O_2 radicals (Anderson et al., 2019). The radical concentration is quantified by reaction with NO, in the absence of ethane, to produce NO_2 that is measured by CAPS. During PROPHET the ECHAMP limit of detection was 1-3 ppt (2σ, 2-min average). Throughout the campaign, the CH_3I calibration method was used as the primary source and the water vapor photolysis method was used less frequently to quantify the relative response of ECHAMP to HO_2 and CH_3O_2 radicals (see below).

As described in Wood et al. (2017) and Kundu et al. (2019), ECHAMP does not detect all peroxy radicals with equal sensitivity. A portion of RO_2 radicals are converted to alkyl nitrites (RONO) and alkyl nitrates ($RONO_2$) via association reactions with NO and a portion of all sampled radicals are lost to wall reactions. Wall loss rate constants measured in the laboratory for halocarbon-coated 0.4 cm ID glass were typically 1.6 s^{-1} for HO_2 at 60% RH and less than 0.2 s^{-1} for CH_3O_2, with isoprene peroxy radical wall loss rate constants between those two values (Kundu et al., 2019). For the sampling conditions during PROPHET (7.3 SLPM flow rate, 13 cm inlet length) this suggests only 2% of HO_2 was lost to wall reactions. Furthermore, an expected 8% of isoprene peroxy radicals are lost to formation of organic nitrates. The relative sensitivity of ECHAMP to HO_2 radicals and CH_3O_2 radicals was quantified after the campaign by comparing its response to both types of radicals prepared at equal concentrations using the water vapor photolysis method. These measurements showed that the response to HO_2 was 2% lower than the instrument response to CH_3O_2. In the absence of sampling losses we would expect that the response to CH_3O_2 would be 10% lower than the response to HO_2 due to formation of CH_3ONO (Wood et al., 2017). These results indicate that sampling losses of HO_2 were more likely 10% and almost equal to the loss of CH_3O_2 due to CH_3ONO formation. Further details of a calibration source comparison between the LIF and ECHAMP instruments are provided in the Supplement.

2.4 Modeling concentrations of OH, HO_2, and XO_2

Ambient concentrations of OH, HO_2, and XO_2 were modelled with the Master Chemical Mechanism (MCM) (Jenkin et al., 1997; Jenkin et al., 2015) and the Regional Atmospheric Chemistry Mechanism version 2 (RACM2) (Goliff et al., 2013). The RACM2 mechanism groups several species according to their reactivity and includes more than 350 reactions. While the near-explicit MCM is expected to better represent the complex oxidation chemistry of this environment, the grouped RACM2 model is more computationally efficient and simpler to use in a radical budget analysis. Due to the limited isoprene oxidation mechanism in the base RACM2 model, a series of reactions described by Tan et al. (2017) was incorporated based on the LIM1 mechanism proposed by Peeters et al. (2009; 2014). The resulting condensed version of LIM1 includes updated bulk reaction rate constants for the 1,6-H shift isomerization reactions of the isoprene peroxy radicals as parameterized by Peeters et al. (2014). These isomerization reactions lead to the formation of HO_2 and hydroperoxyaldehydes (HPALDS) which can photolyze leading to OH production, as well as dihydroperoxy-carbonyl peroxy radicals (di-HPCARPs) which can rapidly decompose to produce additional OH radicals (Teng et al., 2017; Wennberg et al., 2018).

The Master Chemical Mechanism provides a near-explicit mechanism that describes the gas-phase chemical processes involved in the degradation of over 140 VOCs. Model simulations utilized both MCM version 3.2 and MCM version 3.3.1, the latter of which incorporates the explicit LIM1 mechanism and includes the equilibrium between different isoprene peroxy radical

isomers and the H-shift isomerization reactions of specific isomers resulting in HO_x radical recycling through the production of HPALDs as well as di-HPCARP radicals (Jenkin et al., 2015). In this mechanism, the equilibrium rate coefficients between different peroxy radical isomers were increased and the 1,6 H-shift isomerization rate constants were decreased in order to match early experimental results of Crounse et al. (2014) (Peeters, 2015)These changes resulted in effective bulk 1,6 H-shift peroxy radical isomerization rate constants in MCM v3.3.1 that are approximately a factor of 5 lower than the original LIM1 recommended rates (Novelli et al., 2020).

Each of the chemical mechanisms were embedded into the Framework for 0-D Atmospheric Modeling (F0AM) (Wolfe et al., 2016) to calculate radical concentrations predicted by each mechanism. Modeled chemistry for both mechanisms was constrained to measurements of meteorological data and a wide variety of trace gas mixing ratios that were measured during the campaign (Tables S1 and S2). Model simulations were performed with a 30-min integration time and a 5-day spin-up to allow sufficient time to generate unmeasured secondary oxidation products. A 24-h lifetime was assumed for all calculated species to simulate loss via dry deposition and to prevent unexpected accumulation of some unmeasured species. Similar to Ren et al. (2013) and Lu et al. (2012), model sensitivity runs indicate that increasing this depositional loss by a factor of 2 results in changes of the modeled HO_2 concentration of less than 4%. Measurement constraints were synchronized to 30-min time intervals. Species that were measured more frequently were averaged to 30-min intervals, and linear interpolation was used for species measured with lower time resolution.

In cases when speciated measurements or complete measurement sets were not available for species important to radical chemistry, an appropriate correlation analysis, or an average of previous measurements conducted at the PROPHET location were used to constrain the model. For example, measurements of the sum of methyl vinyl ketone and methacrolein (MVK + MACR) were available throughout the campaign from the University of Minnesota's PTR-QiToF instrument, but speciated MACR was measured on some days by the IMT Nord Europe online GC/FID/FID. An MVK:MACR ratio of 0.65:0.35 was derived from a correlation of the available measurements and used to constrain the model when speciated measurements were not available. Similarly, as the sum of monoterpenes was measured by PTR-QiTOF, the mixing ratio of total monoterpenes was constrained as α-pinene in model simulations. Because measurements of HONO concentrations at the top of the tower were unavailable, the model was constrained to the campaign average of previous measurements at this site (Griffith et al., 2013). Photolysis frequencies were calculated using a trigonometric parameterization based on solar zenith angle (Jenkin et al., 1997; Wolfe et al., 2016) and scaled according to measured values of $J(NO_2)$ to account for cloud coverage. The uncertainty of modeled radical concentrations is estimated to be 30% based on uncertainties from model constraint inputs and the measured rate constants for each reaction (Griffith et al., 2013; Wolfe et al., 2016).

In addition to the standard RACM2 and MCM v3.2 models, and the expanded isoprene chemistry in RACM2-LIM1 and MCM v3.3.1, a third set of model simulations were conducted to investigate the influence of $RO_2 + RO_2$ accretion reactions and dimer formation on overall radical concentrations. A set of reactions were added to both RACM2-LIM1 and MCM v3.3.1 to create overall mechanisms (RACM-ACC and MCM-ACC) that incorporate $RO_2 + RO_2$ accretion reactions for both isoprene- and monoterpene-based peroxy radicals. Several studies have reported observations of highly oxidized $C_{19-20}H_{28-32}O_{10-18}$ dimer products in chambers (Ehn et al., 2014) and in field measurements (Yan et al., 2016; Zha et al., 2018), suggesting that RO_2 reactivity in the process of dimer formation increases along with functionalization and size of the RO_2 radical (Berndt et al., 2018a; Berndt et al., 2018b). Rate constants for the added reactions were based on measurements from Berndt et al. (2018a; 2018b) and are intended to represent complex autoxidation and dimer formation chemistry into a model process that results in net radical termination.

Rate constants for several $RO_2 + RO_2$ reactions used in this study are shown in Table 2. As described above, measurements of the sum of all monoterpenes were interpreted as α-pinene in the model and thus rate constants measured in an exclusively α-pinene

system (Berndt et al., 2018a) were used and provide only an estimation of the terpene chemistry at the PROPHET site that also includes emissions of β-pinene, limonene, and others (Carroll et al., 2001; Ortega et al., 2007). In addition to C_{10}-RO_2 radicals derived from monoterpenes, measured rate constants for self- and cross-reactions of C_5-RO_2 radicals derived from isoprene are also included, as well as more general, slower reactions between C_{10}-RO_2 and other smaller RO_2 species. For the purposes of this study, rate constants are based on measurements of the least oxidized C_{10}-RO_2 species described in Berndt et al. (2018a), and thus may represent a lower limit in terms of autooxidation and dimer reactions as a radical sink. As such, the goal of this model was not to provide a detailed mechanism or exact representation of chemistry, but instead to investigate the plausibility of autooxidation and dimer formation and the relative importance that the process may have as a radical termination process in low NO_x, high BVOC environment.

Table 2: Summary of RO_2 + $R'O_2$ → ROOR' rate constants added to RACM-ACC and MCM-ACC based on Berndt et al. (Berndt et al., 2018a; Berndt et al., 2018b)

RO_2	$R'O_2$	k ($cm^3 molecule^{-3} s^{-1}$)
O_3-monoterpene	O_3-monoterpene	9.7×10^{-12}
OH-monoterpene	OH-monoterpene	3.7×10^{-11}
OH-isoprene	OH-isoprene	6.0×10^{-13}
OH-isoprene	OH-monoterpene	1.3×10^{-11}
O_3-monoterpene	other	1.0×10^{-12}
OH-monoterpene	other	2.0×10^{-12}
other	other	$<4.0 \times 10^{-13}$

3 Results

3.1 Meteorological and chemical conditions

A complete suite of supporting measurements, including meteorological conditions and important chemical species that were used as model constraints is shown in Fig. 1, and campaign average measured values of important model constraints are shown in Fig. 2. In general, weather during the campaign was sunny with intermittent clouds, with some exceptions of more overcast days (July 8, 15, 17, 24). Mixing ratios of NO, O_3, and photolysis rate constants were similar to those observed during previous field campaigns at the same site (Griffith et al., 2013). The maximum observed NO mixing ratio was 480 ppt on July 11, and the average peak mixing ratio of NO was approximately 115 ppt at 9:00 local time. NO mixing ratios at night were typically less than 0.5 ppt. Average ozone mixing ratios were between 25 and 35 ppb. Maximum average daytime temperatures of 24 °C were similar to measurements at this site in 2008, but warmer than measurements at this site in 2009, resulting in average mixing ratios of isoprene that peaked near 3 ppb at approximately 18:00, similar to that measured in 2008, but greater than that measured in 2009 (Griffith et al., 2013). These measurements are summarized along with those from previous campaigns at the PROPHET site in Table S3. Mixing ratios of anthropogenic VOCs were low with average mixing ratios of toluene and benzene below 65 and 40 ppt, respectively.

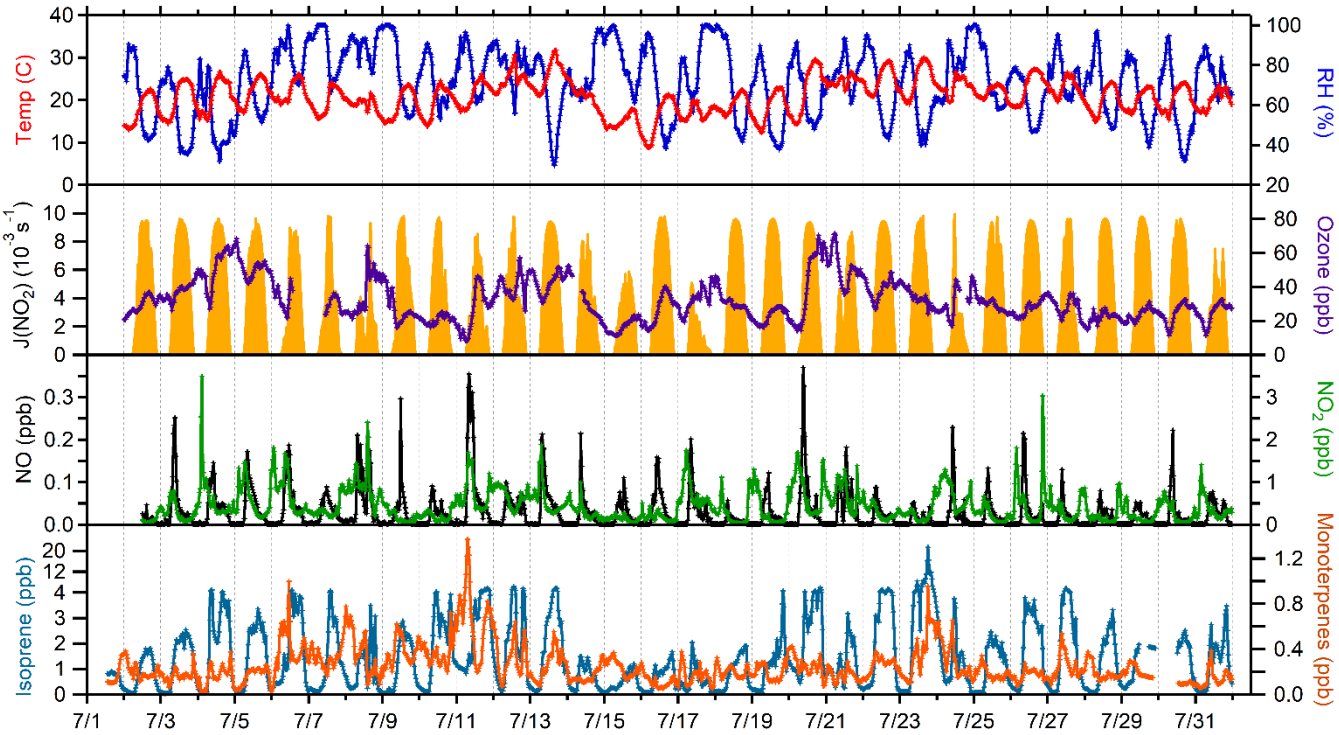

Figure 1: Time series of measured meteorological and chemical conditions used as constraints for model calculations.

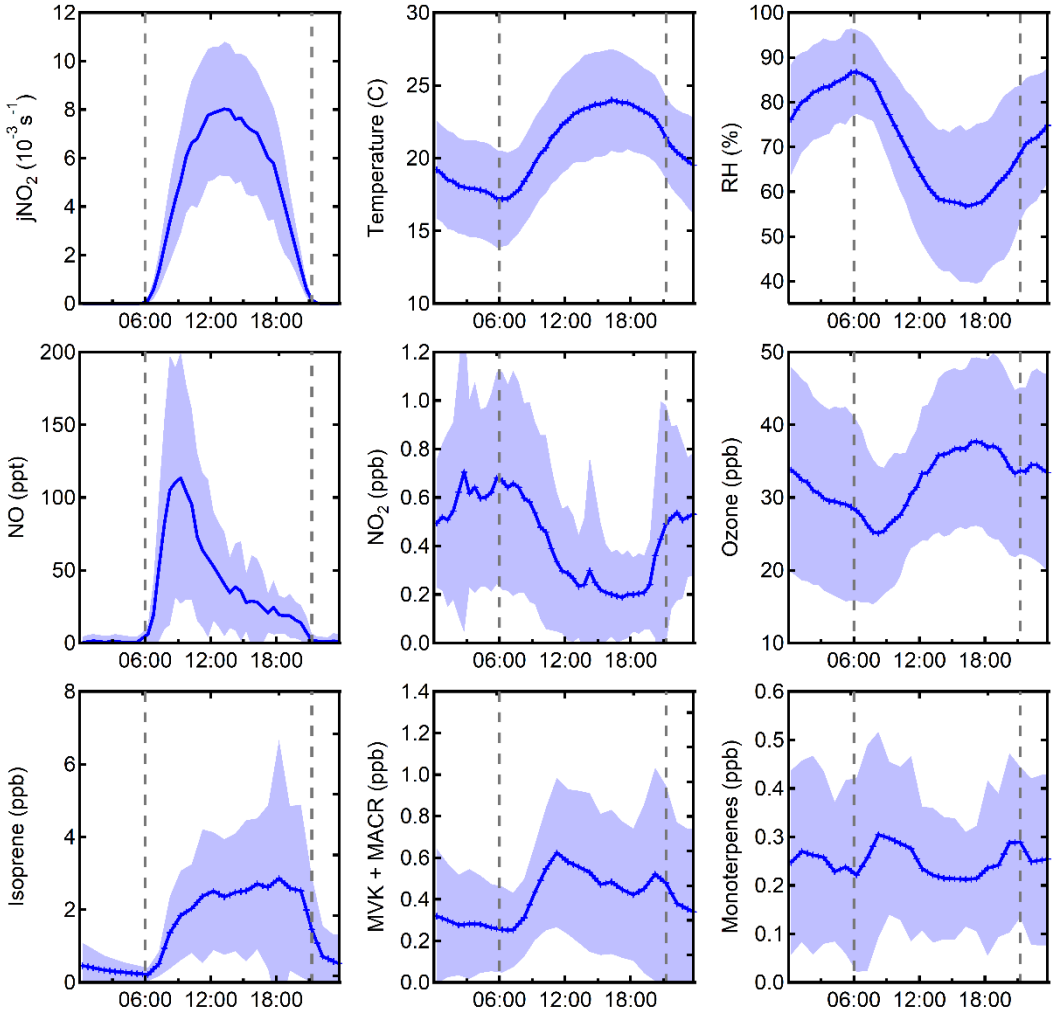

Figure 2: Campaign average measurements of jNO_2, temperature, relative humidity, NO, NO_2, O_3, isoprene, and methyl vinyl ketone and methacrolein. Shaded areas represent the 1σ variability.

3.2 OH measurements and model predictions

Measured and modelled OH, HO_2, and XO_2 concentrations from July 2 through July 31 are shown in Fig. 3 with correlation plots shown in Fig. S2. Measurements of OH were hampered by high background signals and limited laser power. Diurnal profiles with a 2-h time resolution of the OH measurements are shown in Fig. 4, in addition to the model results. An average of all OH measurements performed during the campaign shows a peak of 1.25×10^6 molecules cm^{-3} at 13:00. Measurements of OH during the morning hours were significantly lower than all model calculations. An experimental OH budget based on measured concentrations of OH, HO_2, and other species that contribute to OH production and loss is shown in Fig. S3. The imbalance between 7:00 and 12:00 suggests either a missing OH sink or errors with the OH measurement during this time. The reason for this discrepancy is not clear but may be the result of participant activity on the top of the tower near the detection cell in the mornings during the campaign which may have influenced the OH measurements, although a systematic measurement error during this time cannot be ruled out.

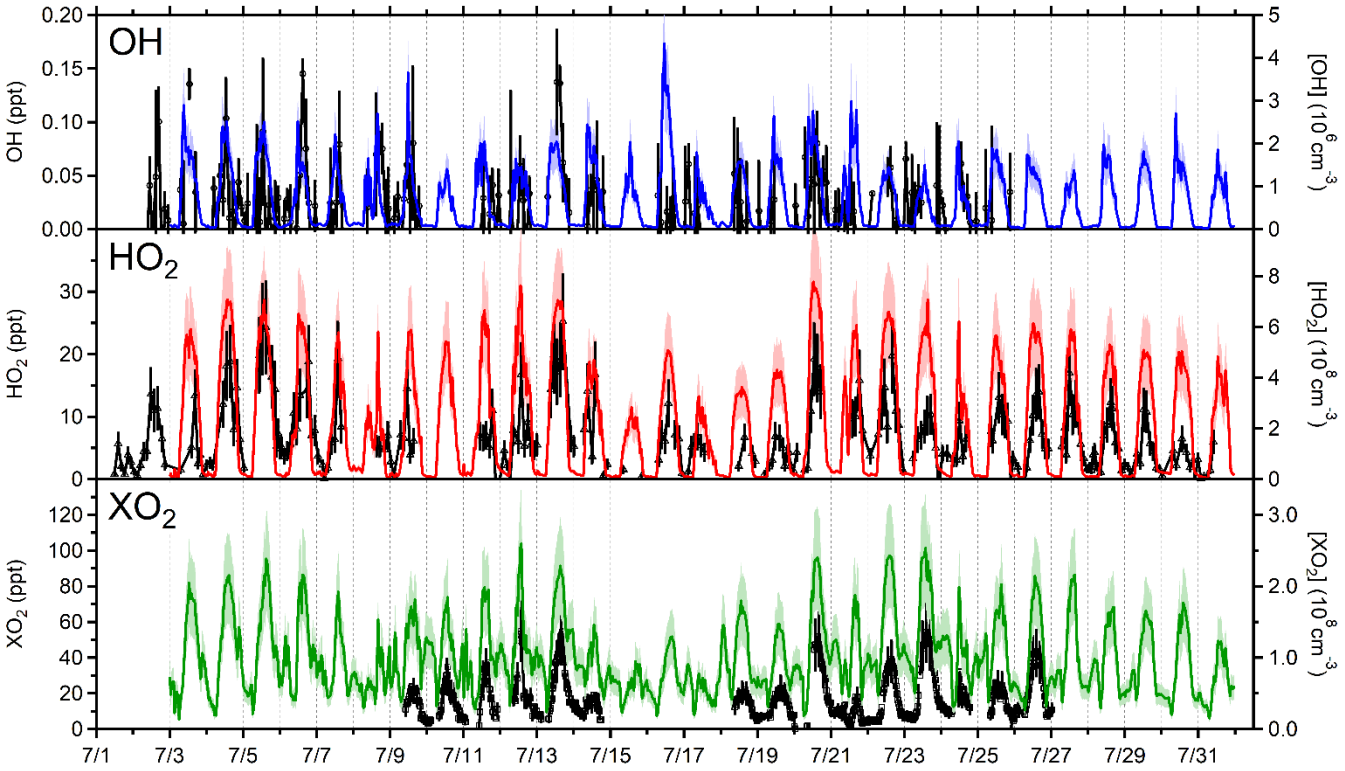

Figure 3: Time series of radical measurements (black) and MCM v3.3.1 model predictions of OH (blue), HO_2 (red), and XO_2 (green) from July 2 to July 31. Measurement of any potential interferences in the OH measurements have been subtracted and only positive OH measurements are shown for simplicity.

Measurements of potential interferences by chemical modulation through addition of C_3F_6 as described above did not reveal any significant unknown interferences, similar to that observed previously at this site (Griffith et al., 2013), but in contrast to measurements by the IU FAGE instrument during the IRRONIC (Indiana Radical, Reactivity and Ozone Production Intercomparison) campaign (Lew et al., 2020). Lew et al. (2020) found that the measured interference increased with both ozone and temperature, similar to that observed by Mao et al. (2012) who also measured a similar interference that increased with both temperature and total OH reactivity. Laboratory studies suggest that the interference could be due to the decomposition of Criegee intermediates inside the low-pressure detection cell leading to OH production (Novelli et al., 2014a; Fuchs et al., 2016; Novelli et al., 2017; Rickly and Stevens, 2018) although estimated concentrations of Criegee intermediates in similar environments are too low to explain the observed interference (Novelli et al., 2017). Another proposed source of the interference is the decomposition of ROOOH molecules inside the FAGE detection cell formed from the reaction of OH with RO_2 radicals (Fittschen et al., 2019). While the sources of these interferences are still unknown, one possible explanation for the absence of a measurable interference during PROPHET-AMOS is the lower measured mixing ratios of ozone and lower temperatures compared to that measured during IRRONIC, resulting in lower mixing ratios of isoprene and other BVOCs. Based on the observed correlation of the interference with ozone and temperature highlighted in Lew et al. (2020), it is likely that a similar interference was undetectable during PROPHET-AMOS.

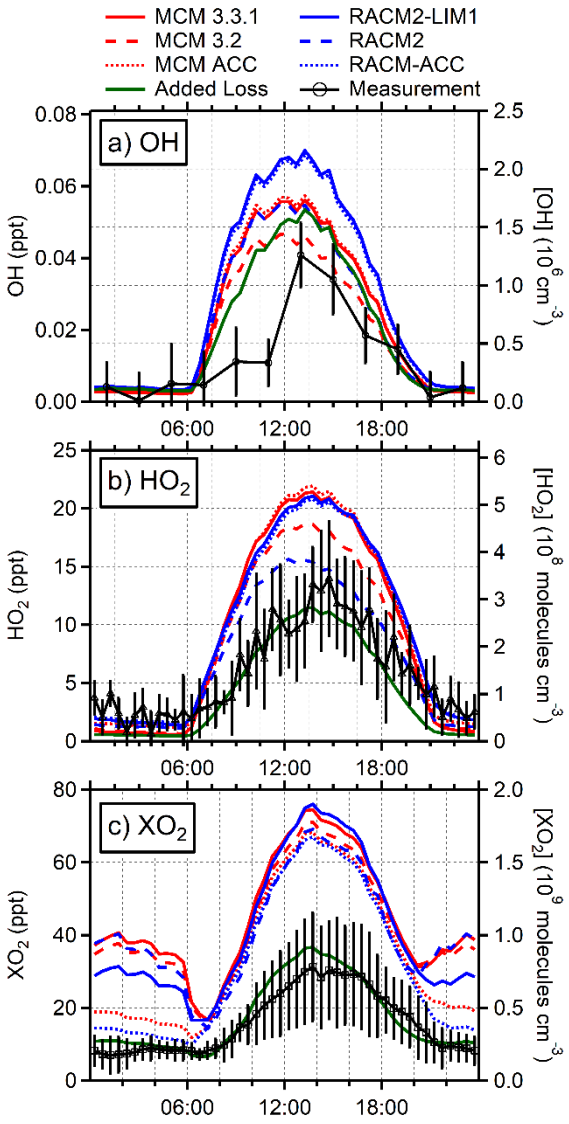

Figure 4: Diurnal average measured (black) and modeled concentrations of (a) OH, (b) HO_2, and (c) XO_2. MCM models are shown in red and RACM2 in blue. The green line represents an additional version of the RACM-ACC model with added sinks for HO_2 and isoprene peroxy radicals. The colored lines represent an average of individual daily model runs from only the days that each respective species was measured (OH: 7/3–7/9, 7/11–7/14, and 7/16–7/25; HO_2: 7/3–7/9 and 7/11–7/31; XO_2: 7/9–7/14 and 7/18–7/26). Error bars represent the 1σ measurement precision.

The measured OH concentrations reported here are similar to previous measurements made by the IU-FAGE instrument at the PROPHET site in 2009 but are lower than those measured at the site in 2008, although the latter measurements suffered from poor precision (Griffith et al., 2013). The results reported here are also in contrast to measurements of OH at this site in 1998 as reported by Tan et al. (2001), who reported maximum daytime concentrations of approximately 4×10^6 cm^{-3} that were approximately a factor of 3 greater than model predictions (Table S3). While the mixing ratios of NO_x and isoprene in 1998 were similar to those observed during PROPHET-AMOS, mixing ratios of ozone were higher in 1998, with the average maximum of approximately 45 ppb similar to that observed during the IRRONIC campaign (Lew et al., 2020). In addition, anomalously elevated concentrations of OH were observed at night in 1998 (Faloona et al., 2001; Tan et al., 2001). These results suggest that the OH measurements in 1998 at the PROPHET site may have been influenced by interferences similar to those observed by Mao et al. (2012), Feiner et al. (2016), and Lew et al. (2020). As illustrated in Fig. 4, the base RACM2 and MCM v3.2 models are able to reproduce the maximum observed OH concentrations to within the combined measurement precision and uncertainty of the models. The addition of LIM1 chemistry to the models increased the predicted average maximum OH concentration by approximately 20% between MCM v3.2

and MCM v3.3.1, and by 30% between RACM2 and RACM2-LIM1, with the MCM v3.3.1 maximum modeled OH concentrations approximately 30% greater than the measured concentrations, and the RACM2-LIM1 maximum modeled OH concentrations approximately 60% greater than the measured concentrations. These results are in contrast to several previous LIF measurements in forested environments (Rohrer et al., 2014), in which measured OH concentrations were significantly higher than modeled predictions. However, the results reported here are similar to that found by Feiner et al. (2016) in an Alabama forest during SOAS (Southern Oxidant and Aerosol Study) where isoprene was the dominant BVOC. In that study, the modeled OH concentrations using MCM v3.3.1 were in good agreement with the measured concentrations when interferences were subtracted from the measurements.

While the predictions by both the RACM2 and MCM models are within the combined uncertainty of the measurements and the models, the MCM v3.3.1 results are in better agreement with the measurements (Fig. 4), which could suggest that the measurements are consistent with the lower effective bulk 1,6-H shift peroxy radical isomerization rate constants in MCM v3.3.1 compared to the original LIM1 recommended rates (Novelli et al., 2020). This is in contrast to the results of from the IRRONIC campaign discussed above, where the MCM v3.3.1 model underpredicted the measured concentrations by approximately a factor of 2, with the RACM2-LIM1 model predictions in better agreement with the measurements (Lew et al., 2020). Similarly, Novelli et al. (2020) reported that the MCM v3.3.1 mechanism underpredicted measurements of OH by a factor of approximately 1.4 during isoprene oxidation experiments in the SAPHIR (Simulation of Atmospheric Photochemistry In a large Reaction) chamber when mixing ratios of NO were less than 0.2 ppb. Unfortunately, the poor precision of the OH measurements reported here do not allow a robust test of the two mechanisms.

3.3 HO_2 and XO_2 measurements and model predictions

The time series of measured and modelled HO_2, and total peroxy radical (XO_2) concentrations from July 2 through July 31 are shown in Fig. 3 and correlation plots of the measured concentrations and MCM v3.3.1 model predictions are shown in Fig. S2. Daily maxima were typically observed between 13:30 and 15:30 local time and ranged from 1.7×10^8 cm^{-3} (6.7 ppt) to 7.0×10^8 cm^{-3} (28.2 ppt) for HO_2 and 2.7×10^8 cm^{-3} (10.8 ppt) to 1.3×10^9 cm^{-3} (52.1 ppt) for XO_2. Measured diurnal average profiles are shown in Fig. 4 along with average model results that consider only the days on which each respective species was measured (7/3–7/9 and 7/11–7/31 for HO_2; 7/9–7/14 and 7/18–7/26 for XO_2). In addition, measured RO_2 mixing ratios (HO_2 measured by LIF subtracted from XO_2 measured by ECHAMP) are compared with modeled RO_2 mixing ratios in Fig. S4. The average maximum (12:00–15:00) of HO_2 measurements performed during the campaign was 2.85×10^8 cm^{-3} (11.6 ppt), while the maximum daytime average of the XO_2 measurements was approximately 7.7×10^8 cm^{-3} (29.0 ppt).

The measured HO_2 concentrations were similar to previous measurements at this site. Median daytime maximum concentrations of HO_2* measured in 2008 were approximately 7×10^8 cm^{-3} (28 ppt), while median daytime maximum concentrations of HO_2* measured in 2009 were approximately 5×10^8 cm^{-3} (20 ppt), with nighttime concentrations below 1×10^8 cm^{-3} (4 ppt) during both years (Griffith et al., 2013). The conversion efficiency of isoprene peroxy radicals to the measured HO_2* concentrations during these studies was estimated to be approximately 90%, suggesting that the measured HO_2* concentrations reflected the sum of HO_2 + isoprene peroxy radicals. Given that isoprene peroxy radicals contribute to approximately 33% of the total peroxy radical concentrations during the daytime, the measured HO_2* concentrations in 2008 and 2009 were greater than HO_2 but less than XO_2 concentrations (Table S3). When compared to 2009, the higher HO_2* concentrations measured in 2008 were likely due to the higher mixing ratios of HCHO observed in 2008 leading to greater rates of radical production (Griffith et al., 2013). The higher mixing ratios of HCHO may be a result of the higher mixing ratios of isoprene leading to a greater production of HCHO during the warmer temperatures observed in 2008 (Griffith et al., 2013).

Average daytime maximum mixing ratios of HO_2 measured at this site in 1998 were reported to be approximately 16 ppt (3.9×10^8 cm^{-3}) with nighttime mixing ratios less than 5 ppt (1.2×10^8 cm^{-3}) (Tan et al., 2001), similar to that measured in this study. However, it is not clear whether the 1998 HO_2 measurements were influenced by interferences from isoprene-based peroxy radicals as discussed above. As a result, these measurements may be an upper limit to the actual HO_2 concentrations. The measured XO_2 concentrations are similar to the total RO_2+HO_2 concentrations measured at this site in 1997 by Mihele and Hastie (2003), who reported daytime maximum mixing ratios between 20 and 65 ppt using a radical chemical amplifier technique, and nighttime mixing ratios of 3–6 ppt. Although not measured at the site during the 1997 campaign, monoterpene mixing ratios observed in 1998, 2008, and 2009 were similar to measurements from 2016 (Table S3).

As illustrated in Fig. 4, the base RACM2 and MCM v3.2 models overpredict both the measured HO_2 and XO_2 concentrations during the daytime, although the agreement with the measured HO_2 concentrations is within the combined uncertainty of the measurements and the model. The base RACM2 model overpredicts the measured average maximum HO_2 concentrations by approximately 30%, while the MCM v3.2 overpredicts the measured daytime maximum HO_2 by approximately 60%. However, including the LIM1 isoprene oxidation mechanism increases the daytime HO_2 concentrations predicted by the base models by approximately 15% and 35% for MCM and RACM2 models, respectively (Fig. 4). Overall, both the RACM2-LIM1 and MCM v3.3.1 models overpredict the measured daytime maximum HO_2 concentrations by approximately 80% which is outside of the combined measurement and model uncertainties. Similarly, the base RACM2 and MCM v3.2 models as well as the updated RACM2-LIM1 and the MCM v3.3.1 models overpredict the daytime XO_2 concentrations by more than a factor of 2, with predicted daytime maximum XO_2 mixing ratios ranging from 65.5 (RACM2) to 72.6 (RACM2-LIM1) ppt (1.6 -1.8×10^9 cm^{-3}).

The model overprediction of the daytime measured HO_2 concentrations is consistent with model simulations of the measured HO_2* concentrations at this site in 2008 and 2009 (Griffith et al., 2013). In 2008, a base RACM model overpredicted the measured HO_2* concentrations by approximately 30% on average, while the same model overpredicted the HO_2* concentrations measured in 2009 by approximately 50%. Similar to the results presented here, addition of the LIM1 mechanism for isoprene oxidation to the RACM model likely would have increased the discrepancy between the 2008 and 2009 measurements. However, these model results are in contrast to that observed at this site in 1998, where a RACM-based model was able to reproduce the reported measured HO_2 concentrations (Tan et al., 2001). As discussed above, these measurements likely represent an upper limit to the actual HO_2 concentrations as it is not clear whether the measurements of HO_2 were free from interferences from isoprene-based and other alkene-based peroxy radicals (Fuchs et al., 2011; Lew et al., 2018). As a result, it is likely that this RACM-based model of Tan et al. (2001) overestimated the actual HO_2 concentrations in 1998. The results reported here are also in contrast to the results of Mihele and Hastie (2003), who found that a 0-D MCM-based model could reproduce the measured daytime XO_2 concentrations on several days. Similarly, these results are in contrast to the IRRONIC campaign, where the MCM and RACM2 models were able to reproduce the measured HO_2* concentrations to within 30% (Lew et al., 2020), as well as the results from SOAS, where the MCM v3.3.1 model was able to reproduce the measured HO_2 concentrations to within the combined uncertainties of the measurement and the model (Feiner et al., 2016). The ability of the models to reproduce the measured peroxy radical concentrations in these studies may reflect the higher mixing ratios of NO_x observed at the PROPHET site in 1997, the SOAS site, and at the IRRONIC site, resulting in a greater contribution of the RO_2 + NO_x reactions to the fate of peroxy radicals during these campaigns (Mihele and Hastie, 2003; Sanchez et al., 2018; Lew et al., 2020). An analysis of the discrepancies between the PROPHET and IRRONIC campaigns will be presented in a subsequent paper.

The composition of the total peroxy radical concentration (XO_2) in the RACM2-LIM1 model is shown in Fig. 5. As illustrated in this figure, the model predicts that HO_2 radicals comprise approximately 33% of the total daytime maximum XO_2 concentration, with isoprene peroxy radicals accounting for approximately 33%, methyl peroxy radicals approximately 12%, acyl

peroxy radicals approximately 7%, and peroxy radicals from alkane, alkene, and terpene oxidation comprising the remaining 15%. Given that the model agreement with the measurements is better for HO_2, the majority of the discrepancy between the modeled and measured XO_2 concentrations is likely due to a greater overestimation of RO_2 radicals, including isoprene-based peroxy radicals. These results are in contrast to that reported by Kundu et al. (2019), who found that their measurements of XO_2 concentrations by the ECHAMP instrument during the IRRONIC campaign could be reproduced on several days by a model incorporating the MCM v3.2 chemical mechanism. As discussed above, the ability of the models to reproduce the measured concentrations during IRRONIC may reflect the higher mixing ratios of NO observed during this campaign, resulting in a greater contribution of $RO_2 + NO_x$ reactions to the fate of peroxy radicals at this site.

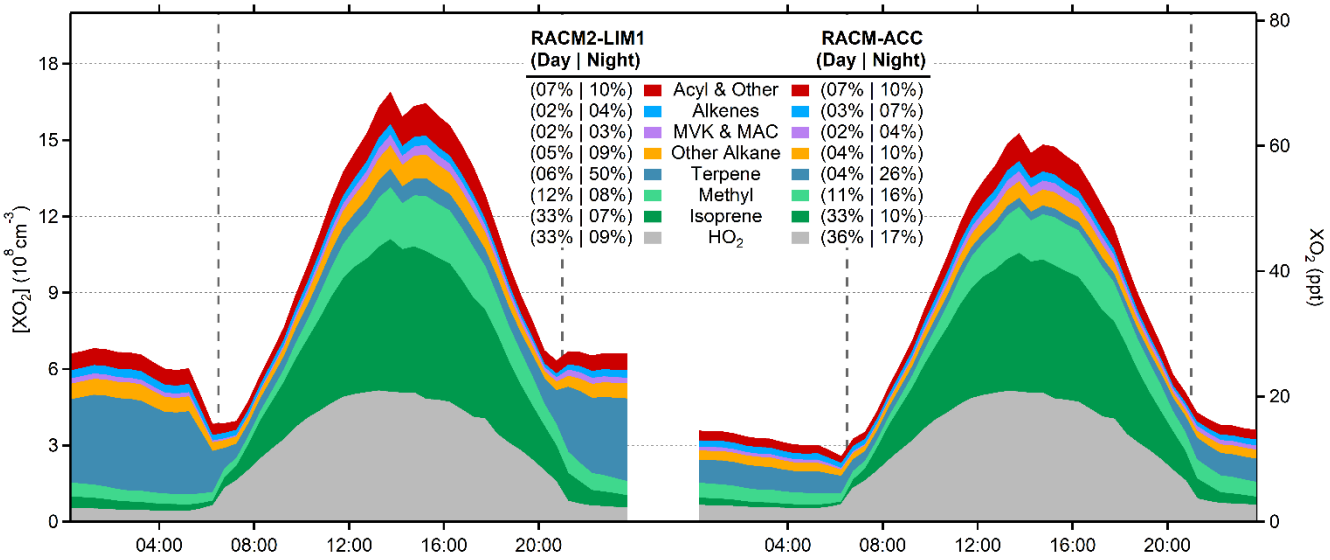

Figure 5: Modeled XO_2 composition from RACM2-LIM1 (left) and RACM-ACC (right). Colors represent peroxy radicals derived from the listed VOCs and numbers represent the percentage contribution of each species to the total concentration of XO_2 during the day (06:30 to 21:00) and at night (21:00 to 06:30), respectively.

During the nighttime, the models reproduce the measured HO_2 concentrations but overestimate the measured XO_2 radical concentrations (Fig. 4). The RACM2 and MCM models overpredict the nighttime XO_2 concentrations by factor of approximately 4, with the RACM2-LIM1 model predicting mixing ratios of total peroxy radicals of approximately 27 ppt between 21:00 and 6:00 and the MCM v3.3.1 model predicting XO_2 mixing ratios of approximately 36 ppt during the night (Fig. 4) compared to the measured concentrations of less than 10 ppt. These results are similar to that from the 1997 PROPHET campaign in which measured nighttime XO_2 mixing ratios of 3–6 ppt were overpredicted by more than a factor of 10 by a model that included reactive terpene emissions (Mihele and Hastie, 2003; Sillman et al., 2002). This is in contrast to the results of Kundu et al. (2019), who found that the MCM v3.2 chemical mechanism could reproduce the measured nighttime XO_2 mixing ratios of less than 10 ppt during the IRRONIC campaign which is likely a result of the elevated NO_x mixing ratios at that site.

The RACM2-LIM1 model predicts that approximately 50% of the nighttime total XO_2 radical concentration is composed of peroxy radicals derived from the ozonolysis of monoterpenes (Fig. 5). As mentioned above, the measured sum of monoterpenes was constrained as α-pinene in all model simulations, resulting in an average monoterpene ozonolysis rate constant that is likely similar to that expected from previous speciated measurements of monoterpenes, including limonene and β-pinene, at this site (Ortega et al., 2007; Kim et al., 2011). However, the average ozonolysis rate constant assumed in the model could represent an upper limit if the monoterpene composition was dominated by species less reactive with ozone (e.g. camphene, cymene) or a lower limit if more reactive terpene species were present (e.g. ocimene, limonene) (Atkinson et al., 1990; Khamaganov and Hites, 2001; Atkinson and Arey, 2003).

The addition of the RO_2 + RO_2 accretion reactions described above to the RACM2-LIM1 and MCM v3.3.1 models (RACM-ACC and MCM-ACC) significantly reduces the predicted XO_2 radical concentrations at night by 50%, lowering the measurement/model discrepancy to less than 5 ppt for the RACM-ACC model. As shown in Fig. 5, this is largely due to a reduction in the concentration of organic peroxy radicals derived from monoterpenes due to the relatively large rate constants for the associated RO_2 + RO_2 accretion reactions (Table 2).

3.4 Radical budget analysis

A radical budget analysis for OH, HO_2, isoprene-based peroxy radicals (ISOP) and total RO_x was conducted to provide information about the processes that drive radical production and the radical loss pathways in this environment and also to highlight the relative importance of the changes in radical chemistry upon the addition of the LIM1 mechanism and accretion reactions. Figure 6a illustrates the campaign average production and loss pathways of OH for the RACM2-LIM1 model. This includes both initiation reactions and propagation steps that produce OH in blue, while termination pathways are shown alongside propagation steps that convert OH to HO_2 or RO_2 in red. The addition of the LIM1 reactions increases the maximum OH production rate at 13:45 by 35% from 2.01 ppb h^{-1} in RACM2, to 2.71 ppb h^{-1} in RACM2-LIM1, primarily due to the isomerization of isoprene peroxy radicals to form HPALDs, which readily photolyze to form OH, and also di-HPCARP radicals, which rapidly decompose to produce additional OH radicals (Peeters et al., 2014; Teng et al., 2017; Wennberg et al., 2018). In the morning (6:45-13:15), RACM2-LIM1 suggests the HO_2 + NO reaction is the dominant source of OH radicals, accounting for 41% of total OH production, and as much as 53% when NO mixing ratios are highest. This decreases to 21% in the afternoon and evening as the NO concentration decreases. Photolytic processes are significant throughout the day, with ozone and HONO photolysis contributing up to 28% and 13% respectively during the day. Ozonolysis of alkenes, primarily monoterpenes, is a minor contributor of up to 6% during the day but is the dominant source of OH at night.

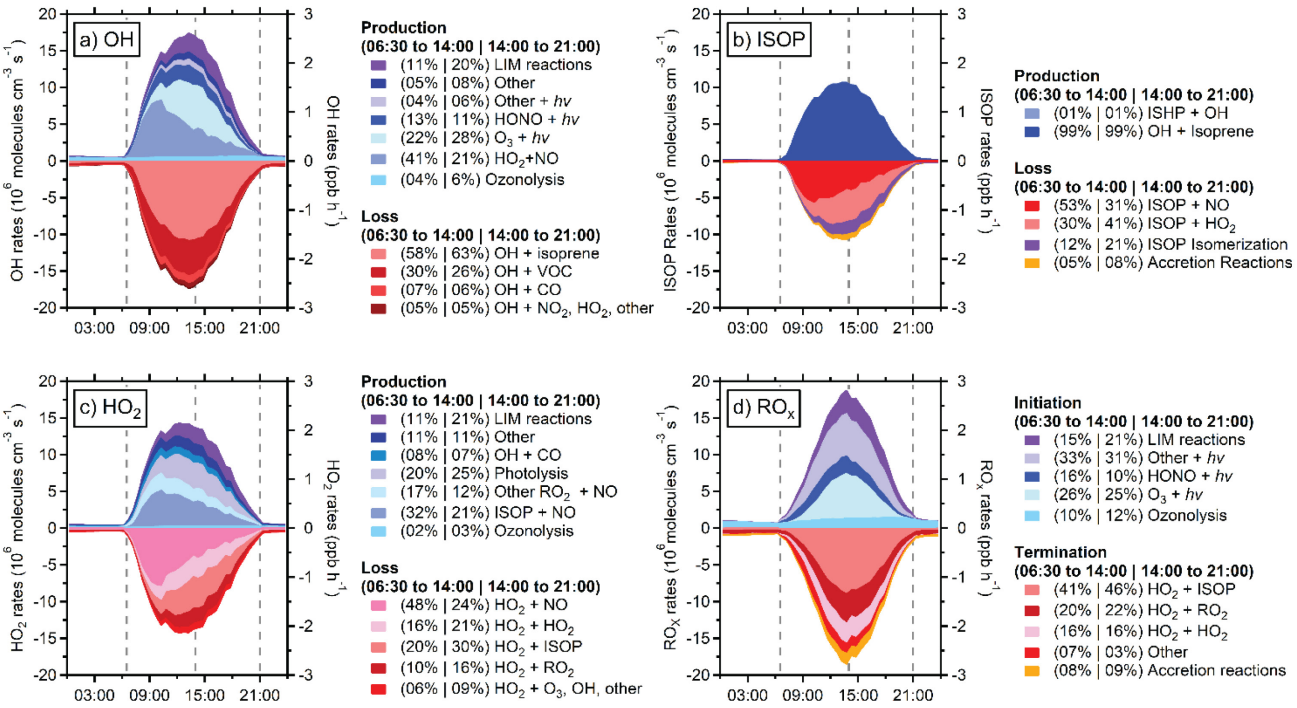

Figure 6: Radical budgets from the RACM2-LIM1 model with additional accretion reactions (RACM-ACC) for a) OH, b) isoprene-based peroxy radicals (ISOP), C) HO_2, and d) total ROx. Shades of blue represent reactions that produce/initiate radicals, and shades of red represent radical loss/termination reactions. LIM reactions (purple) include reactions added as part of the Leuven Isoprene Mechanism. Percentages represent the relative initiation or termination rates of each respective process in the morning (06:30: to 14:00) and during the evening (14:00 to 21:00) which are indicated by the vertical dashed lines.

Reaction with isoprene is the dominant loss pathway for OH radicals accounting for approximately 60% of daytime OH reactivity. Other VOCs (16%), namely monoterpenes, and OVOCs (10%), such as formaldehyde, methyl vinyl ketone, and methacrolein, make up the majority of the remaining daytime OH reactivity. Propagation through reaction with CO is minor (6%), and termination through the OH + NO_2 reaction is not significant (<2%). Consistent with the OH radical budget, the OH + isoprene reaction is the dominant source of isoprene-based peroxy radicals (ISOP; Fig. 6b), with the ISOP + NO reaction accounting for approximately 53% of their total loss in the morning, while the ISOP + HO_2 reaction and peroxy radical isomerization reactions in the LIM1 mechanism account for 62% of isoprene-based peroxy radical loss in the afternoon. The ISOP accretion reaction accounts for only 8% of the loss of isoprene-based peroxy radicals in the afternoon.

Figure 6c illustrates the campaign average HO_2 radical production and loss pathways for RACM2-LIM1. The production of HO_2 in the RACM2-LIM1 model is largely due to turnover from the RO_2 + NO reaction. During the morning, when NO concentrations are greatest, 32% of HO_2 is produced from the reaction of NO and peroxy radicals derived from isoprene while 17% is produced from the reaction of NO with other RO_2 species. In addition to reactions with NO, the photolysis of formaldehyde can account for up to 15% of daytime HO_2 production, and turnover from the OH + CO reaction near 8%. HO_2 loss is primarily due to reaction with NO in the morning (48%) but dominated by the HO_2 self-reaction, reaction with isoprene RO_2 to form ISOPOOH, and reaction with other peroxy radicals in the afternoon and evening (21%, 30%, and 16% respectively).

The total RO_x radical budget is illustrated in Fig. 6d. The addition of LIM1 reactions increases the maximum radical initiation rate by 28% from 2.11 to 2.69 ppb h^{-1}, again primarily due to fast photolysis of HPALDs and decomposition of di-HPCARP radicals. Overall radical initiation in RACM2-LIM1 is largely due to photolytic processes, with a combined 51% from ozone photolysis (26%), HONO (13%), and HPALDs (18%), and 32% from the photolysis of other species such as hydrogen peroxide, aldehydes, organic peroxides, and nitric acid. Ozonolysis is a consistent radical initiation source of approximately 0.21 ppb h^{-1} throughout the day, which dominates RO_x initiation at night and is a significant contributor (11%) throughout the day when photolysis sources are dominant.

Daytime termination of radicals in RACM2-LIM1 is dominated by peroxy radical self- and cross-reactions, primarily the reaction of isoprene peroxy radicals with HO_2 to form ISOPOOH (44%) but also the HO_2 self-reaction (16%) and HO_2 + other RO_2 species (21%). Radical reactions with NO_x were less significant due to the low NO_x concentrations and accounted for at most 0.13 ppb h^{-1}, or less than 8% of the RACM2-LIM1 termination budget when NO_x mixing ratios were highest and less than 3% total during the daytime. The addition of $RO_2 + RO_2$ accretion reactions in the RACM-ACC model provides an alternative pathway that results in a termination rate equivalent to half that of $HO_2 + RO_2$ reactions at night (4.0×10^5 molecules cm^{-3} s^{-1}) and accounts for 30% of total RO_x termination during this time. During the day, when isoprene and NO mixing ratios are higher, these reactions only contribute to 9% of the overall termination due to the lower rate constants for reactions of C_5-RO_2 from isoprene (Table 2). As shown in Fig. 4, this results in better agreement between the measurement and model at night, but model overprediction during the day remains.

4 Discussion

As illustrated in Fig. 4, including the accretion reactions shown in Table 2 into both the RACM2-LIM1 and MCM v3.3.1 models improves the agreement between the model and measured XO_2 concentrations at night to within the combined uncertainty of the model and the measurements, although the agreement of the RACM2 model is better. However, including these accretion reactions in the model only decreases the modeled XO_2 concentrations by 9% during the daytime when isoprene-based peroxy radicals dominate the total XO_2 composition (Fig. 5), as the $RO_2 + RO_2$ accretion rate constants for isoprene-based peroxy radicals are smaller compared to that for monoterpene-based peroxy radicals (Table 2).

One possible explanation for the model discrepancies with the measured HO_2 and XO_2 concentrations during the daytime are errors associated with the measurements of these radicals, such as a systematic error in the calibration of HO_2 or XO_2 radicals. However, as discussed above, measurements of XO_2 concentrations during the IRRONIC campaign were in good agreement with model predictions by the RACM2 and MCM mechanisms, where isoprene dominated OH reactivity during the daytime and isoprene-based peroxy radicals likely contributed to approximately 30% of the total XO_2 concentrations, similar to that observed during PROPHET-AMOS (Kundu et al., 2019). While measurements of HO_2 were not conducted during IRRONIC, the measured HO_2* concentrations were also found to be in good agreement with the model predictions (Lew et al., 2020). In addition, the measured XO_2/HO_2* ratio was found to be in good agreement with the modelled ratio (Kundu et al., 2019). While these results do not rule out the possibility of errors associated with the calibration of the ECHAMP and IU-FAGE instruments, they suggest that the discrepancy between the measurement and model predictions during PROHET-AMOS may not be due to a systematic error in the measurements. As noted in Sect. 2.3, ECHAMP is expected to be 8% less sensitive to isoprene RO_2 than other peroxy radicals. As the modeled isoprene RO_2 mixing ratio accounted for approximately 33% of modeled XO_2 during the daytime (Fig. 5), this suggests that the measured XO_2 represents a lower limit and could be as much as 3% higher than reported. Given the large

differences between modeled and measured XO_2 of more than a factor of two during mid-day, this difference cannot account for the discrepancy with the modeled concentrations.

Measurements of isoprene hydroxy hydroperoxides (ISOPOOH) produced from the reaction of isoprene-based RO_2 radicals with HO_2 can provide an additional test of the model chemistry at this site. Figure 7a shows the average ISOPOOH mixing ratio measured during PROPHET-AMOS between July 22 and July 27 by the Caltech low-pressure GC-CIMS instrument (Vasquez et al., 2018) along with MCM model results. The measured mixing ratios were similar to that observed during the SOAS campaign (Kaiser et al., 2016). The measurements shown include both the 1,2- and 4,3-ISOPOOH isomers, although the 1,2-ISOPOOH constitutes the dominant fraction (Vasquez et al., 2018). In order to achieve a more realistic comparison, a measurement-based deposition term for ISOPOOH and isoprene hydroxy nitrates (IHN) (Nguyen et al., 2015; Wei et al., 2021) was included in the mechanism for all model runs shown in this figure. Still, as illustrated in Fig. 7a, the RACM2-ACC and MCM-ACC models overpredict the measured ISOPOOH concentrations by approximately a factor of 8-10 during the daytime, consistent with the overprediction of peroxy radicals by the models. Constraining the model to the measured concentrations of HO_2 and isoprene-RO_2 (assuming the same relative distribution of RO_2 radicals predicted by the models) improves the agreement (Fig. 7a), although the model still overestimates the measured concentrations. This overestimate of the measured ISOPOOH is similar to that observed during the SOAS campaign (Kaiser et al., 2016), where a large dilution rate was needed to bring the modeled ISOPOOH into agreement with the measurements. Similarly, the model also overestimates the concentrations of IHN produced from the reaction of isoprene peroxy radicals with NO and measured using iodine adduct CIMS (Xiong et al., 2015). Constraining the model to the measured peroxy radical concentrations improves the agreement with the measurements (Fig. 7b). It is also worth noting that the model does not account for losses of IHN due to reactive uptake onto aerosol and subsequent hydrolysis in the aerosol phase (Jacobs et al., 2014; Morales et al., 2021; Wang et al., 2021). Knowledge and incorporation of such loss rates in the model could better constrain the modeled IHN concentrations but the effect is expected to be small in comparison to the adjustment in the modeled output when constrained to measured RO_2. (Wei et al., 2021; Mayhew et al., 2022) These results suggest that the measured HO_2 and XO_2 concentrations are consistent with the measured ISOPOOH and IHN concentrations and that the models are overpredicting the concentrations of HO_2 and isoprene-based peroxy radicals, either through an overestimation of their production or an underestimation of their loss.

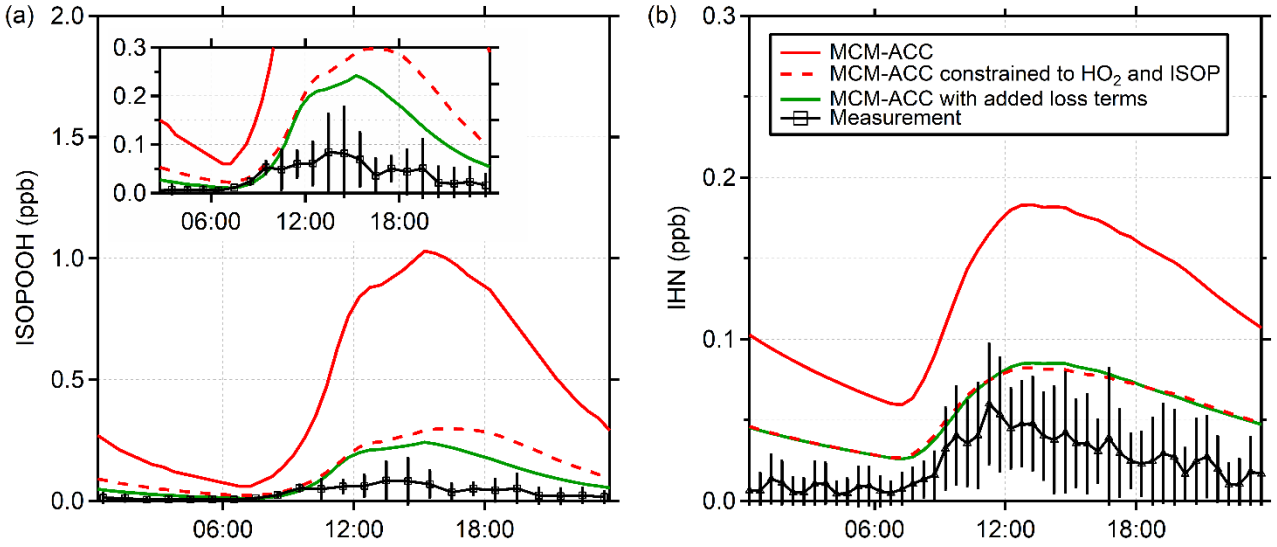

Figure 7: Measured and modelled mixing ratios of (a) isoprene hydroxy hydroperoxides (ISOPOOH) and (b) isoprene hydroxy nitrates (IHN). Measurements of ISOPOOH are an average from July 23-27 (Vasquez et al., 2018) and measurements of IHN are an average of July 6-31. The solid lines represent modeled mixing ratios from MCM-ACC models, The dashed line represents predictions of the same model constrained to measured values of HO_2 and measurements of XO_2 scaled to the modeled isoprene RO_2 composition.

The radical budget analysis suggests that the OH + isoprene reaction is the main source of isoprene-based peroxy radicals during PROPHET-AMOS (Fig. 6b). Measurements of the total OH reactivity together with the measurement of the concentration of OH can provide an estimate of the rate of peroxy radical production from reactions of VOCs with OH. Measurements of total OH reactivity were also conducted during PROPHET-AMOS using both the Indiana University Total OH Loss Method (IU-TOHLM) instrument (Hansen et al., 2014) and the IMT Nord Europe Comparative Reactivity Measurement (CRM) instrument (Hansen et al., 2015), and an analysis of the results and the instrument intercomparison will be presented in a subsequent paper. Figure 8 shows the diurnal averaged total OH reactivity as measured by the IU-TOHLM instrument along with that predicted by the MCM v3.3.1 model. As illustrated in this figure, the measured OH reactivity agreed with that calculated from measured and modeled OH sinks, including the reactivity of some unmeasured oxidation products, suggesting that the loss of OH is well represented by the models. Reaction with isoprene is the dominant daytime OH radical sink, accounting for approximately 60% of the total OH reactivity during the day, in both the MCM v3.3.1 (Fig. 8) and RACM2-LIM1 (Fig. S6) models.

The reasonable agreement between the measured and modeled OH concentrations and total OH reactivity suggests that the rate of production of peroxy radicals by the reaction of OH with isoprene and other VOCs is not overestimated by the model given that these reactions are the dominant source of peroxy radicals during PROPHET-AMOS. In addition, because radical propagation by the RO_2 + NO reaction is a major source of HO_2 radicals, it is unlikely that the model is overestimating the production of HO_2 radicals, although photolysis of HCHO and other aldehydes are also predicted to be a significant source of HO_2 radicals, contributing up to 20-25% of total HO_2 production. However, HCHO and other aldehydes were measured during the campaign, providing a constraint on radical production by the photolysis of these compounds.

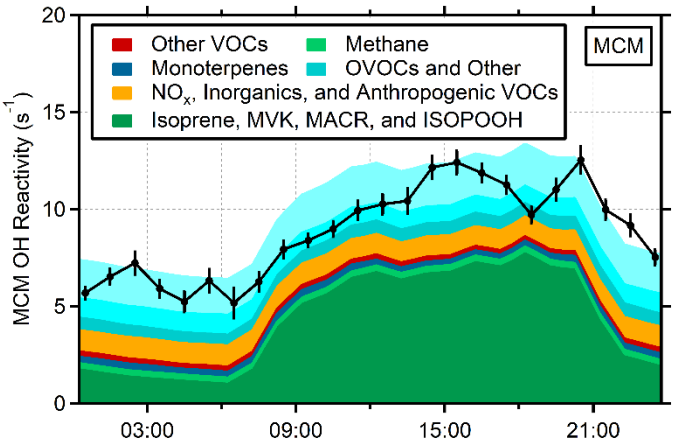

Figure 8: Diurnal average of the measured (IU-TOHLM instrument) and modeled total OH reactivity at the top of the tower during PROPHET-AMOS. Modeled reactivity is largely based on measured species that are used as constraints in the model but also includes contributions from unmeasured oxidation products in the MCM v.3.3.1 model.

Reactant segregation, where unevenly distributed surface flux leads to incomplete mixing in the convective boundary layer, could lead to an effective reduction in the rate of isoprene oxidation by OH, resulting in an overestimation of the reaction rate by the models. While it has been suggested that segregation between OH and isoprene could effectively reduce the rate of the OH + isoprene reaction by 60% (Butler et al., 2008), recent studies have suggested that segregation of OH and isoprene may result in an effective reduction in the rate of the OH + isoprene reaction of less than 15% (Ouwersloot et al., 2011; Pugh et al., 2011). As a result, it is unlikely that reactant segregation is responsible for the discrepancy between the measured and modeled HO_2 and XO_2 concentrations described above, and the overprediction of these peroxy radicals by the models is likely due to an underestimation of radical termination rather than an overestimation of the production of these radicals. An additional loss of HO_2 and isoprene-based RO_2 radicals on the order of the rate of these peroxy radicals with NO is needed in order to resolve the daytime discrepancy between the model and the measurements. Figure 4 includes the results of an additional model that features the RACM2-ACC chemical mechanism but also includes additional sinks for HO_2 and isoprene peroxy radicals (green line in Fig. 4). The added HO_2 sink corresponds to a first-order loss rate of 0.012 s^{-1}, which is approximately 40% of the daytime HO_2 loss, while the added isoprene-based RO_2 sink corresponds to a first-order loss rate of 0.024 s^{-1}, which is approximately 60% of the daytime loss of isoprene-based peroxy radicals (Fig. S5). The addition of these peroxy radical loss mechanisms reduces the predicted daytime maximum OH concentration by 25% to 1.65 × 10^6 cm^{-3}, which is within the combined uncertainties of the measurement and the model (Fig. 4a). These loss processes could potentially include several components, such as uptake of radicals and important precursors to aerosols or the forest canopy, faster self- and cross-reactions between C_5-RO_2 and other RO_2 species that serve as RO_2 radical sinks, or reaction of RO_2 radicals with isoprene or other unsaturated VOCs.

The first-order loss of HO_2 on aerosols can be estimated assuming a first-order loss to aerosol surfaces (Ravishankara, 1997; Whalley et al., 2010) (Eq. 1) where A is the aerosol surface area per volume (cm^2 cm^{-3}), γ is the uptake coefficient, c_g is the mean molecular speed of a gas (cm s^{-1}) given by Eq. 2 where R is the gas constant, T is the temperature and M_w is the molecular weight of the gas. Aerosol uptake coefficients for HO_2 radicals have been measured in both laboratory and field studies, with most values ranging from less than 0.1 to 0.4 (Taketani et al., 2008; Thornton et al., 2008; Taketani et al., 2012; George et al., 2013; Zhou et al., 2021). Assuming values of A = 100 μm^2 cm^{-3} typical of rural aerosols (Cai et al., 2017) and γ = 0.1 results in an estimated first-order loss rate of approximately 0.001 s^{-1}, while assuming values of A = 200 μm^2 cm^{-3} and γ = 0.4 results in an estimated first-order loss of approximately 0.008 s^{-1}. Similar assumptions for isoprene-based peroxy radicals result in an estimated first-order loss of approximately $6 \times 10^{-4} - 5 \times 10^{-3}$ s^{-1}. Assuming an uptake coefficient of γ = 1 for isoprene-based peroxy radicals

would lead to estimated first-order loss rates of approximately $6\times10^{-3} - 1 \times 10^{-2}$ s^{-1}. These results suggest that while heterogeneous loss of peroxy radicals on aerosols may contribute to the model overestimation of the measurements they may not be the only loss mechanism missing in the model.

$$k'_{loss} = \frac{c_g A \gamma}{4}, \quad (2)$$

$$c_g = \sqrt{\frac{8RT}{\pi M_w}}, \quad (3)$$

Recent studies have detected products of the reaction of RO_2 radicals with unsaturated VOCs under atmospheric conditions and suggested that the reaction of isoprene-based peroxy radicals with isoprene could be a significant radical termination reaction in low NO_x regions (NO ≤ 0.05 ppb) (Noziere et al., 2023). Assuming a rate constant of 10^{-14} cm^3 s^{-1} for this reaction based on measurements of the rate of the reaction of acyl peroxy radicals with 2,3-dimethyl-2-butene, the reaction of isoprene-based peroxy radicals with isoprene would result in an estimated first-order loss of approximately 5×10^{-4} s^{-1}. Although this RO_2 + alkene rate coefficient is not large enough to resolve the discrepancy between the measured and modeled XO_2 mixing ratios at the PROPHET site, RO_2 radicals derived from the OH-oxidation of isoprene and monoterpenes could exhibit enhanced reactivity to alkenes and constitute a more significant portion of the missing radical sink (Nozière and Fache, 2021).

An underestimation of radical termination by the reactions of isoprene-based RO_2 radicals could also be responsible for the discrepancies between the modeled and measured peroxy radical concentrations. The overestimation of the measured ISOPOOH concentration by the model (Fig. 7a) suggests that the model is not underestimating the rate of radical termination by the reaction of HO_2 with isoprene-based RO_2 radicals. To account for the missing loss of isoprene-based RO_2 radicals, an accretion rate constant for the self-reaction of isoprene-based RO_2 radicals of approximately 4×10^{-11} cm^3 $molecule^{-1}$ s^{-1}, similar to that for the self-reaction of monoterpene RO_2 radicals (Table 2), would bring the modeled peroxy radical concentrations into agreement with the measurements. While this is greater than the factor of 2-3 uncertainty associated with the measured rate constant for this reaction (Berndt et al., 2018), a combination of loss rates from aerosol uptake, RO_2 reactions with alkenes, and accretion reactions would require a smaller accretion rate constant for isoprene-based RO_2 radicals. An analysis of the experimental radical budgets including the impact of potential additional loss rates will be presented in a subsequent publication.

Another potential loss process in the 0-D model includes vertical and/or horizontal transport of peroxy radicals given their relatively longer modeled lifetimes under the low NO_x conditions at the PROPHET site. The average chemical lifetimes of HO_2 and isoprene-based peroxy radicals during the daytime range from 35–135 s and 40–160 s, respectively. These calculated lifetimes depend primarily on the reactions of HO_2 and isoprene-based RO_2 with the measured radical concentrations and the measured concentration of NO, but also on the reactions of HO_2 with O_3 and the isoprene RO_2 isomerization reactions included in the LIM1 mechanism. These lifetimes are on the order of the expected canopy mixing timescale in forested environments (~2 min) (Wolfe et al., 2011; Wei et al., 2021), suggesting that deposition to the canopy surface could constitute a portion of the missing radical loss process, and could be more significant on well-mixed days. Similar to the above discussion, radical loss to surfaces within the forest canopy can be estimated using Eq. 2 where *A* now represents the ratio of the canopy surface area to the height of the mixing layer. Previous measurements at the PROPHET site reported a leaf area index (LAI) of approximately 3.8 m^2 m^{-2} (Ortega et al., 2007). Assuming a mixing layer height of 1500 m, this suggests that an HO_2 uptake coefficient of $\gamma = 5 \times 10^{-4}$ would result in a first order loss rate of 0.013 s^{-1}, which could account for the proposed missing HO_2 sink. This uptake coefficient is lower than those measured for many atmospheric aerosols but is similar to measurements of HO_2 uptake on organic aerosols (Lakey et al., 2015). Similarly, an uptake coefficient of $\gamma = 1.7 \times 10^{-3}$ for isoprene peroxy radicals would result in a first order loss rate of 0.024 s^{-1} and could account for the missing radical sink. These results imply that loss to surfaces within the canopy could be a substantial

radical loss mechanism in dense forests where low NO_x mixing ratios result in longer peroxy radical lifetimes that are on the order of the transport time through the canopy.

5 Summary

The daytime maximum measured OH radical concentrations during the PROPHET-AMOS campaign were generally in good agreement with model simulations using both the RACM2 and MCM v3.2 chemical mechanisms, though both models overestimated the measured values in the morning. In contrast to previous measurements by the IU-FAGE instrument, no significant OH interferences were measured during the campaign, perhaps due to the lower temperatures and ozone concentrations, which seem to be correlated with unknown interferences associated with the LIF-FAGE technique (Lew et al., 2020). Including the LIM1 isoprene chemical mechanism into the RACM2-LIM1 and MCM v3.3.1 models increases the maximum modeled OH concentration by approximately 30%, with the MCM v3.3.1 mechanism in better agreement with the measurements. These results are in contrast to previous measurements in forest environments, where the measurements were found to be significantly greater than model predictions (Rohrer et al., 2014).

Both the RACM2 and MCM models overpredict the measured daytime concentration of HO_2 by approximately 50% and the measured XO_2 concentrations by approximately a factor of 2, similar to previous measurements at this site (Griffith et al., 2013). During the nighttime, the models are able to reproduce the measured HO_2 concentrations but overestimate the measured XO_2 radical concentrations by factors of approximately 3-5, with approximately 50% of the nighttime total XO_2 radical concentration composed of peroxy radicals derived from the ozonolysis of monoterpenes. The addition of the $RO_2 + RO_2$ accretion reactions to the models significantly reduces the predicted XO_2 radical concentrations at night by up to 60% due to the relatively large rate constants for the $RO_2 + RO_2$ accretion reactions of monoterpene-derived peroxy radicals. However, including these $RO_2 + RO_2$ accretion reactions does not significantly impact the modeled daytime peroxy radical concentrations when isoprene-based peroxy radicals dominate the total XO_2 composition, as the reported $RO_2 + RO_2$ accretion rate constants for isoprene-based peroxy radicals are smaller compared to that for monoterpene-based peroxy radicals.

The models also overpredict the daytime measured concentrations of isoprene hydroxy hydroperoxide and isoprene hydroxy nitrates, consistent with an overprediction of the concentration of isoprene-based peroxy radicals. Constraining the model to the measured peroxy radical concentrations improves the agreement with the measured ISOPOOH and IHN concentrations. These results suggest that the measured radical concentrations are more consistent with the measured ISOPOOH and IHN concentrations, providing additional confidence in the accuracy of the HO_2 and XO_2 radical measurements, and suggest that the model is either overestimating the production of peroxy radicals or, more likely, underestimating their loss. The modeled OH concentrations and total OH reactivity were in good agreement with the measurements, suggesting that the model is not overestimating the production of peroxy radicals, including isoprene-based peroxy radicals.

To reproduce the measured peroxy radical concentrations, an additional loss process equivalent to the reaction of peroxy radicals with NO must be added to the model, accounting for approximately 60% of the total rate of radical termination in the model. The additional loss processes could potentially include several components, such as direct surface deposition of radicals and important precursors to aerosols or the forest canopy, faster self- and cross- reactions between C_5-RO_2 and other RO_2 species, reactions of peroxy radicals with isoprene and other alkenes, or vertical transport of peroxy radicals given their longer lifetime under the low NO_x conditions at the PROPHET site. The overestimation of peroxy radical concentrations suggests that current atmospheric chemistry models may be overestimating the rate of production of ozone and other secondary products in similar low

NO_x areas impacted by isoprene emissions. Additional measurements and modeling studies are needed to resolve these discrepancies.

Data availability. Data presented in this study can be obtained from the authors upon request (pstevens@indiana.edu)

Competing interests. The authors declare that they have no conflicts of interest.

Author contributions. BB, ML, YW, PR, and PSS were responsible for the LIF-FAGE measurements of OH, HO_2, and OH reactivity. BD, MDR, DCA and EW were responsible for the ECHAMP measurements of XO_2. HDA and DBM were responsible for the PTR-MS measurements of VOCs and OVOCs. SD and TL were responsible for the GC measurements of VOCs and OVOCs. AW, GT, JO, and DM were responsible for the measurements of NO and NO_2. WW and DH were responsible for the measurements of O_3 at the Ameriflux tower. JF, ME, and SA were responsible for the measurements of photolysis frequencies and CO. JR, JS, and FK were responsible for the measurements of formaldehyde. HMA was responsible for the measurements of ISOPOOH. JHS and PBS were responsible for the IHN measurements. SB was responsible for coordination and preparation of the PROPHET site. BB, ML, YW, PR, and PSS conducted the analysis and photochemical modelling and wrote the paper with feedback from all co-authors.

Acknowledgements. This study was supported by the National Science Foundation, grants AGS-1440834 and AGS-1827450 to Indiana University, grant AGS-1443842 to the University of Massachusetts Amherst, grant AGS-1719918 to Drexel University, grant AGS-1561755 to the University of Colorado, grant AGS-1643306 to Harvard University, and grants AGS-1932771 and AGS-1428257 to the University of Minnesota. We thank Joe Sakowski for his assistance with the OH, HO_2, and OH reactivity measurements. We also thank Krystal Vasquez, Eric Praske, John Crounse, and Paul Wennberg for their hard effort obtaining the ISOPOOH measurements, Deedee Montzka for assistance in obtaining the NO_x measurements, and all PROPHET-AMOS participants for making this work possible and the University of Michigan Biological Station for hosting the field study.

References

Anderson, D. C., Pavelec, J., Daube, C., Herndon, S. C., Knighton, W. B., Lerner, B. M., Roscioli, J. R., Yacovitch, T. I., and Wood, E. C.: Characterization of ozone production in San Antonio, Texas, using measurements of total peroxy radicals, Atmos. Chem. Phys., 19, 2845-2860, https://doi.org/10.5194/acp-19-2845-2019, 2019.

Atkinson, R. and Arey, J.: Atmospheric Degradation of Volatile Organic Compounds, Chem. Rev., 103, 4605-4638, https://doi.org/10.1021/cr0206420, 2003.

Atkinson, R., Hasegawa, D., and Aschmann, S. M.: Rate constants for the gas-phase reactions of O_3 with a series of monoterpenes and related compounds at 296 ± 2 K, Int. J. Chem. Kinet., 22, 871-887, https://doi.org/10.1002/kin.550220807, 1990.

Badol, C., Borbon, A., Locoge, N., Léonardis, T., and Galloo, J. C.: An automated monitoring system for VOC ozone precursors in ambient air: development, implementation and data analysis, Anal. Bioanal. Chem, 378, 1815-1827, https://doi.org/10.1007/s00216-003-2474-0, 2004.

Baier, B. C., Brune, W. H., Miller, D. O., Blake, D., Long, R., Wisthaler, A., Cantrell, C., Fried, A., Heikes, B., Brown, S., McDuffie, E., Flocke, F., Apel, E., Kaser, L., and Weinheimer, A.: Higher measured than modeled ozone production at increased NO_x levels in the Colorado Front Range, Atmos. Chem. Phys., 17, 11273-11292, https://doi.org/10.5194/acp-17-11273-2017, 2017.

Berndt, T., Mentler, B., Scholz, W., Fischer, L., Herrmann, H., Kulmala, M., and Hansel, A.: Accretion Product Formation from Ozonolysis and OH Radical Reaction of α-Pinene: Mechanistic Insight and the Influence of Isoprene and Ethylene, Environ. Sci. Technol., 52, 11069-11077, https://doi.org/10.1021/acs.est.8b02210, 2018a.

Berndt, T., Scholz, W., Mentler, B., Fischer, L., Herrmann, H., Kulmala, M., and Hansel, A.: Accretion Product Formation from Self- and Cross-Reactions of RO_2 Radicals in the Atmosphere, Angew. Chem. Int. Edit., 57, 3820-3824, https://doi.org/10.1002/anie.201710989, 2018b.

Bianchi, F., Kurtén, T., Riva, M., Mohr, C., Rissanen, M. P., Roldin, P., Berndt, T., Crounse, J. D., Wennberg, P. O., Mentel, T. F., Wildt, J., Junninen, H., Jokinen, T., Kulmala, M., Worsnop, D. R., Thornton, J. A., Donahue, N., Kjaergaard, H. G., and Ehn, M.: Highly Oxygenated Organic Molecules (HOM) from Gas-Phase Autoxidation Involving Peroxy Radicals: A Key Contributor to Atmospheric Aerosol, Chem. Rev., 119, 3472-3509, https://doi.org/10.1021/acs.chemrev.8b00395, 2019.

Bryan, A. M., Cheng, S. J., Ashworth, K., Guenther, A. B., Hardiman, B. S., Bohrer, G., and Steiner, A. L.: Forest-atmosphere BVOC exchange in diverse and structurally complex canopies: 1-D modeling of a mid-successional forest in northern Michigan, Atmos. Environ., 120, 217-226, https://doi.org/10.1016/j.atmosenv.2015.08.094, 2015.

Butler, T. M., Taraborrelli, D., Brühl, C., Fischer, H., Harder, H., Martinez, M., Williams, J., Lawrence, M. G., and Lelieveld, J.: Improved simulation of isoprene oxidation chemistry with the ECHAM5/MESSy chemistry-climate model: lessons from the GABRIEL airborne field campaign, Atmos. Chem. Phys., 8, 4529-4546, https://doi.org/10.5194/acp-8-4529-2008, 2008.

Cai, R., Yang, D., Fu, Y., Wang, X., Li, X., Ma, Y., Hao, J., Zheng, J., and Jiang, J.: Aerosol surface area concentration: a governing factor in new particle formation in Beijing, Atmos. Chem. Phys., 17, 12327-12340, https://doi.org/10.5194/acp-17-12327-2017, 2017.

Cantrell, C. A. and Stedman, D. H.: A possible technique for the measurement of atmospheric peroxy radicals, Geophys. Res. Lett., 9, 846-849, https://doi.org/10.1029/GL009i008p00846, 1982.

Cantrell, C. A., Shetter, R. E., and Calvert, J. G.: Dual-Inlet Chemical Amplifier for Atmospheric Peroxy Radical Measurements, Anal. Chem., 68, 4194-4199, https://doi.org/10.1021/ac960639e, 1996.

Carroll, M. A., Bertman, S. B., and Shepson, P. B.: Overview of the Program for Research on Oxidants: PHotochemistry, Emissions, and Transport (PROPHET) summer 1998 measurements intensive, J. Geophys. Res.- Atmos., 106, 24275-24288, https://doi.org/10.1029/2001JD900189, 2001.

Carslaw, N., Creasey, D. J., Harrison, D., Heard, D. E., Hunter, M. C., Jacobs, P. J., Jenkin, M. E., Lee, J. D., Lewis, A. C., Pilling, M. J., Saunders, S. M., and Seakins, P. W.: OH and HO_2 radical chemistry in a forested region of north-western Greece, Atmos. Environ., 35, 4725-4737, https://doi.org/https://doi.org/10.1016/S1352-2310(01)00089-9, 2001.

Crounse, J. D., Teng, A., and Wennberg, P. O.: Experimental constraints on the distribution and fate of peroxy radicals formed in reactions of isoprene + OH + O_2, presented at Atmospheric Chemical Mechanisms: Simple Models - Real World Complexities, University of California, Davis, USA, 10-12 December, 2014.

Crounse, J. D., Nielsen, L. B., Jørgensen, S., Kjaergaard, H. G., and Wennberg, P. O.: Autoxidation of Organic Compounds in the Atmosphere, J. Phys. Chem. Lett., 4, 3513-3520, https://doi.org/10.1021/jz4019207, 2013.

Crowley, J. N., Pouvesle, N., Phillips, G. J., Axinte, R., Fischer, H., Petäjä, T., Nölscher, A., Williams, J., Hens, K., Harder, H., Martinez-Harder, M., Novelli, A., Kubistin, D., Bohn, B., and Lelieveld, J.: Insights into HO_x and RO_x chemistry in the boreal forest via measurement of peroxyacetic acid, peroxyacetic nitric anhydride (PAN) and hydrogen peroxide, Atmos. Chem. Phys., 18, 13457-13479, https://doi.org/10.5194/acp-18-13457-2018, 2018.

Davis, D. D., Rodgers, M. O., Fischer, S. D., and Asai, K.: An experimental assessment of the O_3/H_2O interference problem in the detection of natural levels of OH via laser induced fluorescence, Geophys. Res. Lett., 8, 69-72, https://doi.org/10.1029/GL008i001p00069, 1981a.

Davis, D. D., Rodgers, M. O., Fischer, S. D., and Heaps, W. S.: A theoretical assessment of the O_3/H_2O interference problem in the detection of natural levels of OH via laser induced fluorescence, Geophys. Res. Lett., 8, 73-76, https://doi.org/10.1029/GL008i001p00073, 1981b.

Dusanter, S., Vimal, D., and Stevens, P. S.: Technical note: Measuring tropospheric OH and HO_2 by laser-induced fluorescence at low pressure. A comparison of calibration techniques, Atmos. Chem. Phys., 8, 321-340, https://doi.org/10.5194/acp-8-321-2008, 2008.

Dusanter, S., Vimal, D., Stevens, P. S., Volkamer, R., and Molina, L. T.: Measurements of OH and HO_2 concentrations during the MCMA-2006 field campaign – Part 1: Deployment of the Indiana University laser-induced fluorescence instrument, Atmos. Chem. Phys., 9, 1665-1685, https://doi.org/10.5194/acp-9-1665-2009, 2009a.

Dusanter, S., Vimal, D., Stevens, P. S., Volkamer, R., Molina, L. T., Baker, A., Meinardi, S., Blake, D., Sheehy, P., Merten, A., Zhang, R., Zheng, J., Fortner, E. C., Junkermann, W., Dubey, M., Rahn, T., Eichinger, B., Lewandowski, P., Prueger, J., and Holder, H.: Measurements of OH and HO_2 concentrations during the MCMA-2006 field campaign – Part 2: Model comparison and radical budget, Atmos. Chem. Phys., 9, 6655-6675, https://doi.org/10.5194/acp-9-6655-2009, 2009b.

Ehn, M., Thornton, J. A., Kleist, E., Sipilä, M., Junninen, H., Pullinen, I., Springer, M., Rubach, F., Tillmann, R., Lee, B., Lopez-Hilfiker, F., Andres, S., Acir, I.-H., Rissanen, M., Jokinen, T., Schobesberger, S., Kangasluoma, J., Kontkanen, J., Nieminen, T., Kurtén, T., Nielsen, L. B., Jørgensen, S., Kjaergaard, H. G., Canagaratna, M., Maso, M. D., Berndt, T., Petäjä, T., Wahner, A., Kerminen, V.-M., Kulmala, M., Worsnop, D. R., Wildt, J., and Mentel, T. F.: A large source of low-volatility secondary organic aerosol, Nature, 506, 476-479, https://doi.org/10.1038/nature13032, 2014.

Faloona, I., Tan, D., Brune, W., Hurst, J., Barket Jr, D., Couch, T. L., Shepson, P., Apel, E., Riemer, D., Thornberry, T., Carroll, M. A., Sillman, S., Keeler, G. J., Sagady, J., Hooper, D., and Paterson, K.: Nighttime observations of anomalously high levels of hydroxyl radicals above a deciduous forest canopy, J. Geophys. Res.- Atmos., 106, 24315-24333, https://doi.org/10.1029/2000JD900691, 2001.

Feiner, P. A., Brune, W. H., Miller, D. O., Zhang, L., Cohen, R. C., Romer, P. S., Goldstein, A. H., Keutsch, F. N., Skog, K. M., Wennberg, P. O., Nguyen, T. B., Teng, A. P., DeGouw, J., Koss, A., Wild, R. J., Brown, S. S., Guenther, A., Edgerton, E., Baumann, K., and Fry, J. L.: Testing Atmospheric Oxidation in an Alabama Forest, J. Atmos. Sci., 73, 4699-4710, https://doi.org/10.1175/JAS-D-16-0044.1, 2016.

Fittschen, C., Al Ajami, M., Batut, S., Ferracci, V., Archer-Nicholls, S., Archibald, A. T., and Schoemaecker, C.: ROOOH: a missing piece of the puzzle for OH measurements in low-NO environments?, Atmos. Chem. Phys., 19, 349-362, https://doi.org/10.5194/acp-19-349-2019, 2019.

Fuchs, H., Bohn, B., Hofzumahaus, A., Holland, F., Lu, K. D., Nehr, S., Rohrer, F., and Wahner, A.: Detection of HO_2 by laser-induced fluorescence: calibration and interferences from RO_2 radicals, Atmos. Meas. Tech., 4, 1209-1225, https://doi.org/10.5194/amt-4-1209-2011, 2011.

Fuchs, H., Tan, Z., Hofzumahaus, A., Broch, S., Dorn, H. P., Holland, F., Künstler, C., Gomm, S., Rohrer, F., Schrade, S., Tillmann, R., and Wahner, A.: Investigation of potential interferences in the detection of atmospheric RO_x radicals by laser-induced fluorescence under dark conditions, Atmos. Meas. Tech., 9, 1431-1447, https://doi.org/10.5194/amt-9-1431-2016, 2016.

Fuchs, H., Hofzumahaus, A., Rohrer, F., Bohn, B., Brauers, T., Dorn, H. P., Häseler, R., Holland, F., Kaminski, M., Li, X., Lu, K., Nehr, S., Tillmann, R., Wegener, R., and Wahner, A.: Experimental evidence for efficient hydroxyl radical regeneration in isoprene oxidation, Nat. Geosci., 6, 1023-1026, https://doi.org/10.1038/ngeo1964, 2013.

George, I. J., Matthews, P. S. J., Whalley, L. K., Brooks, B., Goddard, A., Baeza-Romero, M. T., and Heard, D. E.: Measurements of uptake coefficients for heterogeneous loss of HO_2 onto submicron inorganic salt aerosols, Phys. Chem. Chem. Phys., 15, 12829-12845, https://doi.org/10.1039/C3CP51831K, 2013.

Goliff, W. S., Stockwell, W. R., and Lawson, C. V.: The regional atmospheric chemistry mechanism, version 2, Atmos. Environ., 68, 174-185, https://doi.org/10.1016/j.atmosenv.2012.11.038, 2013.

Griffith, S. M., Hansen, R. F., Dusanter, S., Stevens, P. S., Alaghmand, M., Bertman, S. B., Carroll, M. A., Erickson, M., Galloway, M., Grossberg, N., Hottle, J., Hou, J., Jobson, B. T., Kammrath, A., Keutsch, F. N., Lefer, B. L., Mielke, L. H., O'Brien, A., Shepson, P. B., Thurlow, M., Wallace, W., Zhang, N., and Zhou, X. L.: OH and HO_2 radical chemistry during PROPHET 2008 and CABINEX 2009 - Part 1: Measurements and model comparison, Atmos. Chem. Phys., 13, 5403-5423, https://doi.org/10.5194/acp-13-5403-2013, 2013.

Griffith, S. M., Hansen, R. F., Dusanter, S., Michoud, V., Gilman, J. B., Kuster, W. C., Veres, P. R., Graus, M., de Gouw, J. A., Roberts, J., Young, C., Washenfelder, R., Brown, S. S., Thalman, R., Waxman, E., Volkamer, R., Tsai, C., Stutz, J., Flynn, J. H., Grossberg, N., Lefer, B., Alvarez, S. L., Rappenglueck, B., Mielke, L. H., Osthoff, H. D., and Stevens, P. S.: Measurements of hydroxyl and hydroperoxy radicals during CalNex-LA: Model comparisons and radical budgets, J. Geophys. Res.- Atmos., 121, 4211-4232, https://doi.org/10.1002/2015JD024358, 2016.

Guenther, A. B., Jiang, X., Heald, C. L., Sakulyanontvittaya, T., Duhl, T., Emmons, L. K., and Wang, X.: The Model of Emissions of Gases and Aerosols from Nature version 2.1 (MEGAN2.1): an extended and updated framework for modeling biogenic emissions, Geosci. Model Dev., 5, 1471-1492, https://doi.org/10.5194/gmd-5-1471-2012, 2012.

Hansen, R. F., Blocquet, M., Schoemaecker, C., Léonardis, T., Locoge, N., Fittschen, C., Hanoune, B., Stevens, P. S., Sinha, V., and Dusanter, S.: Intercomparison of the comparative reactivity method (CRM) and pump–probe technique for measuring total OH reactivity in an urban environment, Atmos. Meas. Tech., 8, 4243-4264, https://doi.org/10.5194/amt-8-4243-2015, 2015.

Hansen, R. F., Griffith, S. M., Dusanter, S., Rickly, P. S., Stevens, P. S., Bertman, S. B., Carroll, M. A., Erickson, M. H., Flynn, J. H., Grossberg, N., Jobson, B. T., Lefer, B. L., and Wallace, H. W.: Measurements of total hydroxyl radical reactivity during CABINEX 2009 - Part 1: field measurements, Atmos. Chem. Phys., 14, 2923-2937, https://doi.org/10.5194/acp-14-2923-2014, 2014.

Harley, P., Guenther, A., and Zimmerman, P.: Effects of light, temperature and canopy position on net photosynthesis and isoprene emission from sweetgum (Liquidambar styraciflua) leaves, Tree Physiol., 16, 25-32, https://doi.org/10.1093/treephys/16.1-2.25, 1996.

Hastie, D. R., Weissenmayer, M., Burrows, J. P., and Harris, G. W.: Calibrated chemical amplifier for atmospheric RO_x measurements, Anal. Chem., 63, 2048-2057, https://doi.org/10.1021/ac00018a029, 1991.

Heard, D. E. and Pilling, M. J.: Measurement of OH and HO_2 in the Troposphere, Chem. Rev., 103, 5163-5198, https://doi.org/10.1021/cr020522s, 2003.

Hens, K., Novelli, A., Martinez, M., Auld, J., Axinte, R., Bohn, B., Fischer, H., Keronen, P., Kubistin, D., Nölscher, A. C., Oswald, R., Paasonen, P., Petäjä, T., Regelin, E., Sander, R., Sinha, V., Sipilä, M., Taraborrelli, D., Tatum Ernest, C., Williams, J., Lelieveld, J., and Harder, H.: Observation and modelling of HO_x radicals in a boreal forest, Atmos. Chem. Phys., 14, 8723-8747, https://doi.org/10.5194/acp-14-8723-2014, 2014.

Hofzumahaus, A., Rohrer, F., Lu, K., Bohn, B., Brauers, T., Chang, C.-C., Fuchs, H., Holland, F., Kita, K., Kondo, Y., Li, X., Lou, S., Shao, M., Zeng, L., Wahner, A., and Zhang, Y.: Amplified Trace Gas Removal in the Troposphere, Science, 324, 1702-1704, https://doi.org/10.1126/science.1164566, 2009.

Horstjann, M., Andrés Hernández, M. D., Nenakhov, V., Chrobry, A., and Burrows, J. P.: Peroxy radical detection for airborne atmospheric measurements using absorption spectroscopy of NO_2, Atmos. Meas. Tech., 7, 1245-1257, https://doi.org/10.5194/amt-7-1245-2014, 2014.

Jacobs, M. I., Burke, W. J., and Elrod, M. J.: Kinetics of the reactions of isoprene-derived hydroxynitrates: gas phase epoxide formation and solution phase hydrolysis, Atmos. Chem. Phys., 14, 8933-8946, https://doi.org/10.5194/acp-14-8933-2014, 2014.

Jenkin, M. E., Saunders, S. M., and Pilling, M. J.: The tropospheric degradation of volatile organic compounds: a protocol for mechanism development, Atmos. Environ., 31, 81-104, https://doi.org/10.1016/S1352-2310(96)00105-7, 1997.

Jenkin, M. E., Young, J. C., and Rickard, A. R.: The MCM v3.3.1 degradation scheme for isoprene, Atmos. Chem. Phys., 15, 11433-11459, https://doi.org/10.5194/acp-15-11433-2015, 2015.

Jokinen, T., Sipilä, M., Richters, S., Kerminen, V.-M., Paasonen, P., Stratmann, F., Worsnop, D., Kulmala, M., Ehn, M., Herrmann, H., and Berndt, T.: Rapid Autoxidation Forms Highly Oxidized RO_2 Radicals in the Atmosphere, Angew. Chem. Int. Edit., 53, 14596-14600, https://doi.org/10.1002/anie.201408566, 2014.

Kaiser, J., Skog, K. M., Baumann, K., Bertman, S. B., Brown, S. B., Brune, W. H., Crounse, J. D., de Gouw, J. A., Edgerton, E. S., Feiner, P. A., Goldstein, A. H., Koss, A., Misztal, P. K., Nguyen, T. B., Olson, K. F., St. Clair, J. M., Teng, A. P., Toma, S., Wennberg, P. O., Wild, R. J., Zhang, L., and Keutsch, F. N.: Speciation of OH reactivity above the canopy of an isoprene-dominated forest, Atmos. Chem. Phys., 16, 9349-9359, https://doi.org/10.5194/acp-16-9349-2016, 2016.

Kanaya, Y., Cao, R., Akimoto, H., Fukuda, M., Komazaki, Y., Yokouchi, Y., Koike, M., Tanimoto, H., Takegawa, N., and Kondo, Y.: Urban photochemistry in central Tokyo: 1. Observed and modeled OH and HO_2 radical concentrations during the winter and summer of 2004, J. Geophys. Res.- Atmos., 112, https://doi.org/10.1029/2007JD008670, 2007a.

Kanaya, Y., Cao, R., Kato, S., Miyakawa, Y., Kajii, Y., Tanimoto, H., Yokouchi, Y., Mochida, M., Kawamura, K., and Akimoto, H.: Chemistry of OH and HO_2 radicals observed at Rishiri Island, Japan, in September 2003: Missing daytime sink of HO_2 and positive nighttime correlations with monoterpenes, J. Geophys. Res.- Atmos., 112, https://doi.org/10.1029/2006JD007987, 2007b.

Kanaya, Y., Hofzumahaus, A., Dorn, H. P., Brauers, T., Fuchs, H., Holland, F., Rohrer, F., Bohn, B., Tillmann, R., Wegener, R., Wahner, A., Kajii, Y., Miyamoto, K., Nishida, S., Watanabe, K., Yoshino, A., Kubistin, D., Martinez, M., Rudolf, M., Harder, H., Berresheim, H., Elste, T., Plass-Dülmer, C., Stange, G., Kleffmann, J., Elshorbany, Y., and Schurath, U.: Comparisons of observed and modeled OH and HO_2 concentrations during the ambient measurement period of the HO_xComp field campaign, Atmos. Chem. Phys., 12, 2567-2585, https://doi.org/10.5194/acp-12-2567-2012, 2012.

Khamaganov, V. G. and Hites, R. A.: Rate Constants for the Gas-Phase Reactions of Ozone with Isoprene, α- and β-Pinene, and Limonene as a Function of Temperature, J. Phys. Chem. A, 105, 815-822, https://doi.org/10.1021/jp002730z, 2001.

Kim, S., Guenther, A., Karl, T., and Greenberg, J.: Contributions of primary and secondary biogenic VOC tototal OH reactivity during the CABINEX (Community Atmosphere-Biosphere INteractions Experiments)-09 field campaign, Atmos. Chem. Phys., 11, 8613-8623, https://doi.org/10.5194/acp-11-8613-2011, 2011.

Kim, S., Wolfe, G. M., Mauldin, L., Cantrell, C., Guenther, A., Karl, T., Turnipseed, A., Greenberg, J., Hall, S. R., Ullmann, K., Apel, E., Hornbrook, R., Kajii, Y., Nakashima, Y., Keutsch, F. N., DiGangi, J. P., Henry, S. B., Kaser, L., Schnitzhofer, R., Graus, M., Hansel, A., Zheng, W., and Flocke, F. F.: Evaluation of HO_x sources and cycling using measurement-constrained model calculations in a 2-methyl-3-butene-2-ol (MBO) and monoterpene (MT) dominated ecosystem, Atmos. Chem. Phys., 13, 2031-2044, https://doi.org/10.5194/acp-13-2031-2013, 2013.

Kubistin, D., Harder, H., Martinez, M., Rudolf, M., Sander, R., Bozem, H., Eerdekens, G., Fischer, H., Gurk, C., Klüpfel, T., Königstedt, R., Parchatka, U., Schiller, C. L., Stickler, A., Taraborrelli, D., Williams, J., and Lelieveld, J.: Hydroxyl

radicals in the tropical troposphere over the Suriname rainforest: comparison of measurements with the box model MECCA, Atmos. Chem. Phys., 10, 9705-9728, https://doi.org/10.5194/acp-10-9705-2010, 2010.

Kundu, S., Deming, B. L., Lew, M. M., Bottorff, B. P., Rickly, P., Stevens, P. S., Dusanter, S., Sklaveniti, S., Leonardis, T., Locoge, N., and Wood, E. C.: Peroxy radical measurements by ethane – nitric oxide chemical amplification and laser-induced fluorescence during the IRRONIC field campaign in a forest in Indiana, Atmos. Chem. Phys., 19, 9563-9579, https://doi.org/10.5194/acp-19-9563-2019, 2019.

Lakey, P. S. J., George, I. J., Whalley, L. K., Baeza-Romero, M. T., and Heard, D. E.: Measurements of the HO_2 Uptake Coefficients onto Single Component Organic Aerosols, Environ. Sci. Technol., 49, 4878-4885, https://doi.org/10.1021/acs.est.5b00948, 2015.

Lelieveld, J., Butler, T. M., Crowley, J. N., Dillon, T. J., Fischer, H., Ganzeveld, L., Harder, H., Lawrence, M. G., Martinez, M., Taraborrelli, D., and Williams, J.: Atmospheric oxidation capacity sustained by a tropical forest, Nature, 452, 737-740, https://doi.org/10.1038/nature06870, 2008.

Lew, M. M., Dusanter, S., and Stevens, P. S.: Measurement of interferences associated with the detection of the hydroperoxy radical in the atmosphere using laser-induced fluorescence, Atmos. Meas. Tech., 11, 95-109, https://doi.org/10.5194/amt-11-95-2018, 2018.

Lew, M. M., Rickly, P. S., Bottorff, B. P., Reidy, E., Sklaveniti, S., Léonardis, T., Locoge, N., Dusanter, S., Kundu, S., Wood, E., and Stevens, P. S.: OH and HO_2 radical chemistry in a midlatitude forest: measurements and model comparisons, Atmos. Chem. Phys., 20, 9209-9230, https://doi.org/10.5194/acp-20-9209-2020, 2020.

Lightfoot, P. D., Cox, R. A., Crowley, J. N., Destriau, M., Hayman, G. D., Jenkin, M. E., Moortgat, G. K., and Zabel, F.: Organic peroxy radicals: Kinetics, spectroscopy and tropospheric chemistry, Atmos. Environ. A-Gen., 26, 1805-1961, https://doi.org/10.1016/0960-1686(92)90423-I, 1992.

Liu, Z., Nguyen, V. S., Harvey, J., Müller, J.-F., and Peeters, J.: Theoretically derived mechanisms of HPALD photolysis in isoprene oxidation, Phys. Chem. Chem. Phys., 19, 9096-9106, https://doi.org/10.1039/C7CP00288B, 2017.

Lu, K. D., Hofzumahaus, A., Holland, F., Bohn, B., Brauers, T., Fuchs, H., Hu, M., Häseler, R., Kita, K., Kondo, Y., Li, X., Lou, S. R., Oebel, A., Shao, M., Zeng, L. M., Wahner, A., Zhu, T., Zhang, Y. H., and Rohrer, F.: Missing OH source in a suburban environment near Beijing: observed and modelled OH and HO_2 concentrations in summer 2006, Atmos. Chem. Phys., 13, 1057-1080, https://doi.org/10.5194/acp-13-1057-2013, 2013.

Lu, K. D., Rohrer, F., Holland, F., Fuchs, H., Bohn, B., Brauers, T., Chang, C. C., Häseler, R., Hu, M., Kita, K., Kondo, Y., Li, X., Lou, S. R., Nehr, S., Shao, M., Zeng, L. M., Wahner, A., Zhang, Y. H., and Hofzumahaus, A.: Observation and modelling of OH and HO_2 concentrations in the Pearl River Delta 2006: a missing OH source in a VOC rich atmosphere, Atmos. Chem. Phys., 12, 1541-1569, https://doi.org/10.5194/acp-12-1541-2012, 2012.

Mallik, C., Tomsche, L., Bourtsoukidis, E., Crowley, J. N., Derstroff, B., Fischer, H., Hafermann, S., Hüser, I., Javed, U., Keßel, S., Lelieveld, J., Martinez, M., Meusel, H., Novelli, A., Phillips, G. J., Pozzer, A., Reiffs, A., Sander, R., Taraborrelli, D., Sauvage, C., Schuladen, J., Su, H., Williams, J., and Harder, H.: Oxidation processes in the eastern Mediterranean atmosphere: evidence from the modelling of HO_x measurements over Cyprus, Atmos. Chem. Phys., 18, 10825-10847, https://doi.org/10.5194/acp-18-10825-2018, 2018.

Mao, J., Ren, X., Zhang, L., Van Duin, D. M., Cohen, R. C., Park, J. H., Goldstein, A. H., Paulot, F., Beaver, M. R., Crounse, J. D., Wennberg, P. O., DiGangi, J. P., Henry, S. B., Keutsch, F. N., Park, C., Schade, G. W., Wolfe, G. M., Thornton, J. A., and Brune, W. H.: Insights into hydroxyl measurements and atmospheric oxidation in a California forest, Atmos. Chem. Phys., 12, 8009-8020, https://doi.org/10.5194/acp-12-8009-2012, 2012.

Mayhew, A. W., Lee, B. H., Thornton, J. A., Bannan, T. J., Brean, J., Hopkins, J. R., Lee, J. D., Nelson, B. S., Percival, C., Rickard, A. R., Shaw, M. D., Edwards, P. M., and Hamilton, J. F.: Evaluation of isoprene nitrate chemistry in detailed chemical mechanisms, Atmos. Chem. Phys., 22, 14783-14798, https://doi.org/10.5194/acp-22-14783-2022, 2022.

Medeiros, D. J., Blitz, M. A., Seakins, P. W., and Whalley, L. K.: Direct Measurements of Isoprene Autoxidation: Pinpointing Atmospheric Oxidation in Tropical Forests, JACS Au, 2, 809-818, https://doi.org/10.1021/jacsau.1c00525, 2022.

Mihele, C. M. and Hastie, D. R.: Optimized Operation and Calibration Procedures for Radical Amplifier-Type Detectors, J. Atmos. Ocean. Tech., 17, 788-794, https://doi.org/10.1175/1520-0426(2000)017<0788:OOACPF>2.0.CO;2, 2000.

Mihele, C. M. and Hastie, D. R.: Radical chemistry at a forested continental site: Results from the PROPHET 1997 campaign, J. Geophys. Res.- Atmos., 108, 4450, https://doi.org/10.1029/2002JD002888, 2003.

Millet, D. B., Alwe, H. D., Chen, X., Deventer, M. J., Griffis, T. J., Holzinger, R., Bertman, S. B., Rickly, P. S., Stevens, P. S., Léonardis, T., Locoge, N., Dusanter, S., Tyndall, G. S., Alvarez, S. L., Erickson, M. H., and Flynn, J. H.: Bidirectional Ecosystem–Atmosphere Fluxes of Volatile Organic Compounds Across the Mass Spectrum: How Many Matter?, ACS Earth Space Chem., 2, 764-777, https://doi.org/10.1021/acsearthspacechem.8b00061, 2018.

Morales, A. C., Jayarathne, T., Slade, J. H., Laskin, A., and Shepson, P. B.: The production and hydrolysis of organic nitrates from OH radical oxidation of β-ocimene, Atmos. Chem. Phys., 21, 129-145, https://doi.org/10.5194/acp-21-129-2021, 2021.

Nguyen, T. B., Crounse, J. D., Teng, A. P., St. Clair, J. M., Paulot, F., Wolfe, G. M., and Wennberg, P. O.: Rapid deposition of oxidized biogenic compounds to a temperate forest, Proc. Natl. Acad. Sci. U.S.A., 112, E392-E401, https://doi.org/10.1073/pnas.1418702112, 2015.

Noell, A. C., Alconcel, L. S., Robichaud, D. J., Okumura, M., and Sander, S. P.: Near-Infrared Kinetic Spectroscopy of the HO_2 and $C_2H_5O_2$ Self-Reactions and Cross Reactions, J. Phys. Chem. A, 114, 6983-6995, https://doi.org/10.1021/jp912129j, 2010.

Novelli, A., Vereecken, L., Lelieveld, J., and Harder, H.: Direct observation of OH formation from stabilised Criegee intermediates, Phys. Chem. Chem. Phys., 16, 19941-19951, https://doi.org/10.1039/C4CP02719A, 2014a.

Novelli, A., Hens, K., Tatum Ernest, C., Kubistin, D., Regelin, E., Elste, T., Plass-Dülmer, C., Martinez, M., Lelieveld, J., and Harder, H.: Characterisation of an inlet pre-injector laser-induced fluorescence instrument for the measurement of atmospheric hydroxyl radicals, Atmos. Meas. Tech., 7, 3413-3430, https://doi.org/10.5194/amt-7-3413-2014, 2014b.

Novelli, A., Hens, K., Tatum Ernest, C., Martinez, M., Nölscher, A. C., Sinha, V., Paasonen, P., Petäjä, T., Sipilä, M., Elste, T., Plass-Dülmer, C., Phillips, G. J., Kubistin, D., Williams, J., Vereecken, L., Lelieveld, J., and Harder, H.: Estimating the atmospheric concentration of Criegee intermediates and their possible interference in a FAGE-LIF instrument, Atmos. Chem. Phys., 17, 7807-7826, https://doi.org/10.5194/acp-17-7807-2017, 2017.

Novelli, A., Vereecken, L., Bohn, B., Dorn, H. P., Gkatzelis, G. I., Hofzumahaus, A., Holland, F., Reimer, D., Rohrer, F., Rosanka, S., Taraborrelli, D., Tillmann, R., Wegener, R., Yu, Z., Kiendler-Scharr, A., Wahner, A., and Fuchs, H.: Importance of isomerization reactions for OH radical regeneration from the photo-oxidation of isoprene investigated in the atmospheric simulation chamber SAPHIR, Atmos. Chem. Phys., 20, 3333-3355, https://doi.org/10.5194/acp-20-3333-2020, 2020.

Nozière, B. and Fache, F.: Reactions of organic peroxy radicals, RO_2, with substituted and biogenic alkenes at room temperature: unsuspected sinks for some RO_2 in the atmosphere?, Chem. Sci., 12, 11676-11683, https://doi.org/10.1039/D1SC02263F, 2021.

Orlando, J. J. and Tyndall, G. S.: Laboratory studies of organic peroxy radical chemistry: an overview with emphasis on recent issues of atmospheric significance, Chem. Soc. Rev., 41, 6294-6317, https://doi.org/10.1039/C2CS35166H, 2012.

Ortega, J., Helmig, D., Guenther, A., Harley, P., Pressley, S., and Vogel, C.: Flux estimates and OH reaction potential of reactive biogenic volatile organic compounds (BVOCs) from a mixed northern hardwood forest, Atmos. Environ., 41, 5479-5495, https://doi.org/https://doi.org/10.1016/j.atmosenv.2006.12.033, 2007.

Ouwersloot, H. G., Vilà-Guerau de Arellano, J., van Heerwaarden, C. C., Ganzeveld, L. N., Krol, M. C., and Lelieveld, J.: On the segregation of chemical species in a clear boundary layer over heterogeneous land surfaces, Atmos. Chem. Phys., 11, 10681-10704, https://doi.org/10.5194/acp-11-10681-2011, 2011.

Owen, S. M., Harley, P., Guenther, A., and Hewitt, C. N.: Light dependency of VOC emissions from selected Mediterranean plant species, Atmos. Environ., 36, 3147-3159, https://doi.org/10.1016/S1352-2310(02)00235-2, 2002.

Peeters, J.: Interactive comment on "The MCM v3.3 degradation scheme for isoprene" by M.E. Jenkin et al., Atmospheric Chemistry and Physics Discussions, 15, C2486, https://doi.org/available at: https://acp.copernicus.org/preprints/15/C2486/2015/acpd-15-C2486-2015-supplement.pdf, 2015.

Peeters, J., Nguyen, T. L., and Vereecken, L.: HO_x radical regeneration in the oxidation of isoprene, Phys. Chem. Chem. Phys., 11, 5935-5939, https://doi.org/10.1039/B908511D, 2009.

Peeters, J., Müller, J.-F., Stavrakou, T., and Nguyen, V. S.: Hydroxyl Radical Recycling in Isoprene Oxidation Driven by Hydrogen Bonding and Hydrogen Tunneling: The Upgraded LIM1 Mechanism, J. Phys. Chem. A, 118, 8625-8643, https://doi.org/10.1021/jp5033146, 2014.

Pugh, T. A. M., MacKenzie, A. R., Langford, B., Nemitz, E., Misztal, P. K., and Hewitt, C. N.: The influence of small-scale variations in isoprene concentrations on atmospheric chemistry over a tropical rainforest, Atmos. Chem. Phys., 11, 4121-4134, https://doi.org/10.5194/acp-11-4121-2011, 2011.

Ravishankara, A. R.: Heterogeneous and Multiphase Chemistry in the Troposphere, Science, 276, 1058-1065, https://doi.org/10.1126/science.276.5315.1058, 1997.

Ren, X., Harder, H., Martinez, M., Lesher, R. L., Oliger, A., Simpas, J. B., Brune, W. H., Schwab, J. J., Demerjian, K. L., He, Y., Zhou, X., and Gao, H.: OH and HO_2 Chemistry in the urban atmosphere of New York City, Atmos. Environ., 37, 3639-3651, https://doi.org/10.1016/S1352-2310(03)00459-X, 2003.

Ren, X., Brune, W. H., Oliger, A., Metcalf, A. R., Simpas, J. B., Shirley, T., Schwab, J. J., Bai, C., Roychowdhury, U., Li, Y., Cai, C., Demerjian, K. L., He, Y., Zhou, X., Gao, H., and Hou, J.: OH, HO_2, and OH reactivity during the PMTACS–NY Whiteface Mountain 2002 campaign: Observations and model comparison, J. Geophys. Res.- Atmos., 111, D10S03, https://doi.org/10.1029/2005JD006126, 2006.

Ren, X., van Duin, D., Cazorla, M., Chen, S., Mao, J., Zhang, L., Brune, W. H., Flynn, J. H., Grossberg, N., Lefer, B. L., Rappenglück, B., Wong, K. W., Tsai, C., Stutz, J., Dibb, J. E., Thomas Jobson, B., Luke, W. T., and Kelley, P.: Atmospheric oxidation chemistry and ozone production: Results from SHARP 2009 in Houston, Texas, J. Geophys. Res.-Atmos., 118, 5770-5780, https://doi.org/10.1002/jgrd.50342, 2013.

Rickly, P. and Stevens, P. S.: Measurements of a potential interference with laser-induced fluorescence measurements of ambient OH from the ozonolysis of biogenic alkenes, Atmos. Meas. Tech., 11, 1-16, https://doi.org/10.5194/amt-11-1-2018, 2018.

Ridley, B. and Grahek, F.: A Small, Low Flow, High Sensitivity Reaction Vessel for NO Chemiluminescence Detectors, J. Atmos. Ocean. Tech., 7, 307-311, https://doi.org/10.1175/1520-0426(1990)007<0307:ASLFHS>2.0.CO;2, 1990.

Rohrer, F., Lu, K., Hofzumahaus, A., Bohn, B., Brauers, T., Chang, C.-C., Fuchs, H., Häseler, R., Holland, F., Hu, M., Kita, K., Kondo, Y., Li, X., Lou, S., Oebel, A., Shao, M., Zeng, L., Zhu, T., Zhang, Y., and Wahner, A.: Maximum efficiency in

the hydroxyl-radical-based self-cleansing of the troposphere, Nat. Geosci., 7, 559-563, https://doi.org/10.1038/ngeo2199, 2014.

Roukos, J., Plaisance, H., Leonardis, T., Bates, M., and Locoge, N.: Development and validation of an automated monitoring system for oxygenated volatile organic compounds and nitrile compounds in ambient air, J. Chromatogr. A, 1216, 8642-8651, https://doi.org/10.1016/j.chroma.2009.10.018, 2009.

Sanchez, D., Jeong, D., Seco, R., Wrangham, I., Park, J.-H., Brune, W. H., Koss, A., Gilman, J., de Gouw, J., Misztal, P., Goldstein, A., Baumann, K., Wennberg, P. O., Keutsch, F. N., Guenther, A., and Kim, S.: Intercomparison of OH and OH reactivity measurements in a high isoprene and low NO environment during the Southern Oxidant and Aerosol Study (SOAS), Atmos. Environ., 174, 227-236, https://doi.org/10.1016/j.atmosenv.2017.10.056, 2018.

Shetter, R. E. and Müller, M.: Photolysis frequency measurements using actinic flux spectroradiometry during the PEM-Tropics mission: Instrumentation description and some results, J. Geophys. Res.- Atmos., 104, 5647-5661, https://doi.org/10.1029/98JD01381, 1999.

Shirley, T. R., Brune, W. H., Ren, X., Mao, J., Lesher, R., Cardenas, B., Volkamer, R., Molina, L. T., Molina, M. J., Lamb, B., Velasco, E., Jobson, T., and Alexander, M.: Atmospheric oxidation in the Mexico City Metropolitan Area (MCMA) during April 2003, Atmos. Chem. Phys., 6, 2753-2765, https://doi.org/10.5194/acp-6-2753-2006, 2006.

Sillman, S., Carroll, M. A., Thornberry, T., Lamb, B. K., Westberg, H., Brune, W. H., Faloona, I., Tan, D., Shepson, P. B., Sumner, A. L., Hastie, D. R., Mihele, C. M., Apel, E. C., Riemer, D. D., and Zika, R. G.: Loss of isoprene and sources of nighttime OH radicals at a rural site in the United States: Results from photochemical models, J. Geophys. Res.- Atmos., 107, ACH 2-1-ACH 2-14, https://doi.org/https://doi.org/10.1029/2001JD000449, 2002.

Sindelarova, K., Granier, C., Bouarar, I., Guenther, A., Tilmes, S., Stavrakou, T., Müller, J. F., Kuhn, U., Stefani, P., and Knorr, W.: Global data set of biogenic VOC emissions calculated by the MEGAN model over the last 30 years, Atmos. Chem. Phys., 14, 9317-9341, https://doi.org/10.5194/acp-14-9317-2014, 2014.

Taketani, F., Kanaya, Y., and Akimoto, H.: Kinetics of Heterogeneous Reactions of HO_2 Radical at Ambient Concentration Levels with $(NH_4)_2SO_4$ and NaCl Aerosol Particles, J. Phys. Chem. A, 112, 2370-2377, https://doi.org/10.1021/jp0769936, 2008.

Taketani, F., Kanaya, Y., Pochanart, P., Liu, Y., Li, J., Okuzawa, K., Kawamura, K., Wang, Z., and Akimoto, H.: Measurement of overall uptake coefficients for HO_2 radicals by aerosol particles sampled from ambient air at Mts. Tai and Mang (China), Atmos. Chem. Phys., 12, 11907-11916, https://doi.org/10.5194/acp-12-11907-2012, 2012.

Tan, D., Faloona, I., Simpas, J. B., Brune, W., Shepson, P. B., Couch, T. L., Sumner, A. L., Carroll, M. A., Thornberry, T., Apel, E., Riemer, D., and Stockwell, W.: HO_x budgets in a deciduous forest: Results from the PROPHET summer 1998 campaign, J. Geophys. Res.- Atmos., 106, 24407-24427, https://doi.org/10.1029/2001JD900016, 2001.

Tan, Z., Lu, K., Hofzumahaus, A., Fuchs, H., Bohn, B., Holland, F., Liu, Y., Rohrer, F., Shao, M., Sun, K., Wu, Y., Zeng, L., Zhang, Y., Zou, Q., Kiendler-Scharr, A., Wahner, A., and Zhang, Y.: Experimental budgets of OH, HO_2, and RO_2 radicals and implications for ozone formation in the Pearl River Delta in China 2014, Atmos. Chem. Phys., 19, 7129-7150, https://doi.org/10.5194/acp-19-7129-2019, 2019.

Tan, Z., Fuchs, H., Lu, K., Hofzumahaus, A., Bohn, B., Broch, S., Dong, H., Gomm, S., Häseler, R., He, L., Holland, F., Li, X., Liu, Y., Lu, S., Rohrer, F., Shao, M., Wang, B., Wang, M., Wu, Y., Zeng, L., Zhang, Y., Wahner, A., and Zhang, Y.: Radical chemistry at a rural site (Wangdu) in the North China Plain: observation and model calculations of OH, HO_2 and RO_2 radicals, Atmos. Chem. Phys., 17, 663-690, https://doi.org/10.5194/acp-17-663-2017, 2017.

Tan, Z., Rohrer, F., Lu, K., Ma, X., Bohn, B., Broch, S., Dong, H., Fuchs, H., Gkatzelis, G. I., Hofzumahaus, A., Holland, F., Li, X., Liu, Y., Liu, Y., Novelli, A., Shao, M., Wang, H., Wu, Y., Zeng, L., Hu, M., Kiendler-Scharr, A., Wahner, A., and Zhang, Y.: Wintertime photochemistry in Beijing: observations of RO_x radical concentrations in the North China Plain during the BEST-ONE campaign, Atmos. Chem. Phys., 18, 12391-12411, https://doi.org/10.5194/acp-18-12391-2018, 2018.

Teng, A. P., Crounse, J. D., and Wennberg, P. O.: Isoprene Peroxy Radical Dynamics, Journal of the American Chemical Society, 139, 5367-5377, https://doi.org/10.1021/jacs.6b12838, 2017.

Thornton, J. A., Jaeglé, L., and McNeill, V. F.: Assessing known pathways for HO_2 loss in aqueous atmospheric aerosols: Regional and global impacts on tropospheric oxidants, J. Geophys. Res.- Atmos., 113, D05303, https://doi.org/10.1029/2007JD009236, 2008.

Tyndall, G. S., Cox, R. A., Granier, C., Lesclaux, R., Moortgat, G. K., Pilling, M. J., Ravishankara, A. R., and Wallington, T. J.: Atmospheric chemistry of small organic peroxy radicals, J. Geophys. Res.- Atmos., 106, 12157-12182, https://doi.org/10.1029/2000JD900746, 2001.

Vasquez, K. T., Allen, H. M., Crounse, J. D., Praske, E., Xu, L., Noelscher, A. C., and Wennberg, P. O.: Low-pressure gas chromatography with chemical ionization mass spectrometry for quantification of multifunctional organic compounds in the atmosphere, Atmos. Meas. Tech., 11, 6815-6832, https://doi.org/10.5194/amt-11-6815-2018, 2018.

Wang, Y., Piletic, I. R., Takeuchi, M., Xu, T., France, S., and Ng, N. L.: Synthesis and Hydrolysis of Atmospherically Relevant Monoterpene-Derived Organic Nitrates, Environ. Sci. Technol., 55, 14595-14606, https://doi.org/10.1021/acs.est.1c05310, 2021.

Wei, D., Alwe, H. D., Millet, D. B., Bottorff, B., Lew, M., Stevens, P. S., Shutter, J. D., Cox, J. L., Keutsch, F. N., Shi, Q., Kavassalis, S. C., Murphy, J. G., Vasquez, K. T., Allen, H. M., Praske, E., Crounse, J. D., Wennberg, P. O., Shepson, P. B., Bui, A. A. T., Wallace, H. W., Griffin, R. J., May, N. W., Connor, M., Slade, J. H., Pratt, K. A., Wood, E. C., Rollings,

M., Deming, B. L., Anderson, D. C., and Steiner, A. L.: FORest Canopy Atmosphere Transfer (FORCAsT) 2.0: model updates and evaluation with observations at a mixed forest site, Geosci. Model Dev., 14, 6309-6329, https://doi.org/10.5194/gmd-14-6309-2021, 2021.

Wennberg, P. O., Bates, K. H., Crounse, J. D., Dodson, L. G., McVay, R. C., Mertens, L. A., Nguyen, T. B., Praske, E., Schwantes, R. H., Smarte, M. D., St Clair, J. M., Teng, A. P., Zhang, X., and Seinfeld, J. H.: Gas-Phase Reactions of Isoprene and Its Major Oxidation Products, Chem. Rev., 118, 3337-3390, https://doi.org/10.1021/acs.chemrev.7b00439, 2018.

Whalley, L. K., Blitz, M. A., Desservettaz, M., Seakins, P. W., and Heard, D. E.: Reporting the sensitivity of laser-induced fluorescence instruments used for HO_2 detection to an interference from RO_2 radicals and introducing a novel approach that enables HO_2 and certain RO_2 types to be selectively measured, Atmos. Meas. Tech., 6, 3425-3440, https://doi.org/10.5194/amt-6-3425-2013, 2013.

Whalley, L. K., Furneaux, K. L., Goddard, A., Lee, J. D., Mahajan, A., Oetjen, H., Read, K. A., Kaaden, N., Carpenter, L. J., Lewis, A. C., Plane, J. M. C., Saltzman, E. S., Wiedensohler, A., and Heard, D. E.: The chemistry of OH and HO_2 radicals in the boundary layer over the tropical Atlantic Ocean, Atmos. Chem. Phys., 10, 1555-1576, https://doi.org/10.5194/acp-10-1555-2010, 2010.

Whalley, L. K., Edwards, P. M., Furneaux, K. L., Goddard, A., Ingham, T., Evans, M. J., Stone, D., Hopkins, J. R., Jones, C. E., Karunaharan, A., Lee, J. D., Lewis, A. C., Monks, P. S., Moller, S. J., and Heard, D. E.: Quantifying the magnitude of a missing hydroxyl radical source in a tropical rainforest, Atmos. Chem. Phys., 11, 7223-7233, https://doi.org/10.5194/acp-11-7223-2011, 2011.

Whalley, L. K., Slater, E. J., Woodward-Massey, R., Ye, C., Lee, J. D., Squires, F., Hopkins, J. R., Dunmore, R. E., Shaw, M., Hamilton, J. F., Lewis, A. C., Mehra, A., Worrall, S. D., Bacak, A., Bannan, T. J., Coe, H., Percival, C. J., Ouyang, B., Jones, R. L., Crilley, L. R., Kramer, L. J., Bloss, W. J., Vu, T., Kotthaus, S., Grimmond, S., Sun, Y., Xu, W., Yue, S., Ren, L., Acton, W. J. F., Hewitt, C. N., Wang, X., Fu, P., and Heard, D. E.: Evaluating the sensitivity of radical chemistry and ozone formation to ambient VOCs and NO_x in Beijing, Atmos. Chem. Phys., 21, 2125-2147, https://doi.org/10.5194/acp-21-2125-2021, 2021.

Wolfe, G. M., Marvin, M. R., Roberts, S. J., Travis, K. R., and Liao, J.: The Framework for 0-D Atmospheric Modeling (F0AM) v3.1, Geosci. Model Dev., 9, 3309-3319, https://doi.org/10.5194/gmd-9-3309-2016, 2016.

Wolfe, G. M., Thornton, J. A., Bouvier-Brown, N. C., Goldstein, A. H., Park, J. H., McKay, M., Matross, D. M., Mao, J., Brune, W. H., LaFranchi, B. W., Browne, E. C., Min, K. E., Wooldridge, P. J., Cohen, R. C., Crounse, J. D., Faloona, I. C., Gilman, J. B., Kuster, W. C., de Gouw, J. A., Huisman, A., and Keutsch, F. N.: The Chemistry of Atmosphere-Forest Exchange (CAFE) Model – Part 2: Application to BEARPEX-2007 observations, Atmos. Chem. Phys., 11, 1269-1294, https://doi.org/10.5194/acp-11-1269-2011, 2011.

Wood, E. C. and Charest, J. R.: Chemical Amplification - Cavity Attenuated Phase Shift Spectroscopy Measurements of Atmospheric Peroxy Radicals, Anal. Chem., 86, 10266-10273, https://doi.org/10.1021/ac502451m, 2014.

Wood, E. C., Deming, B. L., and Kundu, S.: Ethane-Based Chemical Amplification Measurement Technique for Atmospheric Peroxy Radicals, Environ. Sci. Tech. Let., 4, 15-19, https://doi.org/10.1021/acs.estlett.6b00438, 2017.

Xiong, F., McAvey, K. M., Pratt, K. A., Groff, C. J., Hostetler, M. A., Lipton, M. A., Starn, T. K., Seeley, J. V., Bertman, S. B., Teng, A. P., Crounse, J. D., Nguyen, T. B., Wennberg, P. O., Misztal, P. K., Goldstein, A. H., Guenther, A. B., Koss, A. R., Olson, K. F., de Gouw, J. A., Baumann, K., Edgerton, E. S., Feiner, P. A., Zhang, L., Miller, D. O., Brune, W. H., and Shepson, P. B.: Observation of isoprene hydroxynitrates in the southeastern United States and implications for the fate of NO_x, Atmos. Chem. Phys., 15, 11257-11272, https://doi.org/10.5194/acp-15-11257-2015, 2015.

Yan, C., Nie, W., Äijälä, M., Rissanen, M. P., Canagaratna, M. R., Massoli, P., Junninen, H., Jokinen, T., Sarnela, N., Häme, S. A. K., Schobesberger, S., Canonaco, F., Yao, L., Prévôt, A. S. H., Petäjä, T., Kulmala, M., Sipilä, M., Worsnop, D. R., and Ehn, M.: Source characterization of highly oxidized multifunctional compounds in a boreal forest environment using positive matrix factorization, Atmos. Chem. Phys., 16, 12715-12731, https://doi.org/10.5194/acp-16-12715-2016, 2016.

Zha, Q., Yan, C., Junninen, H., Riva, M., Sarnela, N., Aalto, J., Quéléver, L., Schallhart, S., Dada, L., Heikkinen, L., Peräkylä, O., Zou, J., Rose, C., Wang, Y., Mammarella, I., Katul, G., Vesala, T., Worsnop, D. R., Kulmala, M., Petäjä, T., Bianchi, F., and Ehn, M.: Vertical characterization of highly oxygenated molecules (HOMs) below and above a boreal forest canopy, Atmos. Chem. Phys., 18, 17437-17450, https://doi.org/10.5194/acp-18-17437-2018, 2018.

Zhou, J., Sato, K., Bai, Y., Fukusaki, Y., Kousa, Y., Ramasamy, S., Takami, A., Yoshino, A., Nakayama, T., Sadanaga, Y., Nakashima, Y., Li, J., Murano, K., Kohno, N., Sakamoto, Y., and Kajii, Y.: Kinetics and impacting factors of HO_2 uptake onto submicron atmospheric aerosols during the 2019 Air QUAlity Study (AQUAS) in Yokohama, Japan, Atmos. Chem. Phys., 21, 12243-12260, https://doi.org/10.5194/acp-21-12243-2021, 2021.